University of Glasgow

Wetzel, C. et al. (2017) Small-molecule inhibition of STOML3 oligomerization reverses pathological mechanical hypersensitivity. Nature Neuroscience, 20(2), pp. 209-218.

There may be differences between this version and the published version. You are advised to consult the publisher's version if you wish to cite from it.

http://eprints.gla.ac.uk/228926/

Deposited on: 18 January 2021

Enlighten – Research publications by members of the University of Glasgow
http://eprints.gla.ac.uk

Small molecule inhibition of STOML3 oligomerization reverses pathological mechanical hypersensitivity

Christiane Wetzel[1,‡], Simone Pifferi[1,†], Cristina Picci[1,3], Caglar Gök[1], Diana Hoffmann[1,4], Kiran K. Bali[5], André Lampe[6], Liudmila Lapatsina[1], Raluca Fleischer[1], Ewan St. John Smith[1,7], Valérie Bégay[1], Mirko Moroni[1], Luc Estebanez[1,4], Johannes Kühnemund[1], Jan Walcher[1], Edgar Specker[6], Martin Neuenschwander[6], Jens Peter von Kries[6], Volker Haucke[6], Rohini Kuner[5], James F.A. Poulet[1,4], Jan Schmoranzer[8], Kate Poole[1,2,*,‡], Gary R. Lewin[1,4*]

[1]Department of Neuroscience, Max Delbrück Center for Molecular Medicine, Robert-Rössle Straße 10, D-13092 Berlin, Germany,

[2]Department of Physiology and EMBL Australia Node for Single Molecule Science, School of Medical Sciences, UNSW, Sydney, Australia

[3]Department of Biomedical Sciences, Section of Cytomorphology, University of Cagliari, Monserrato (CA), Italy

[4]Neuroscience Research Center and Cluster of Excellence NeuroCure, Charité-Universitätsmedizin, Charitéplatz 1, 10117 Berlin Germany.

[5]Institute of Pharmacology, Heidelberg University, Im Neuenheimer Feld 584, D-69120 Heidelberg, Germany

[6]Leibniz-Institut für Molekulare Pharmakologie (FMP), Robert-Roessle-Str. 10, 13125 Berlin, Germany,

[7]Dept. of Pharmacology, University of Cambridge, Tennis Court Rd., Cambridge, CB2 1PD

[8]Freie Universität Berlin, Robert-Roessle-Straße 10, 13125 Berlin, Germany

[†] Present address: Neurobiology Group, SISSA, International School for Advanced Studies, Via Bonomea 265, 34136 Trieste, Italy

[‡] These authors contributed equally to this work

*Correspondence to: glewin@mdc-berlin.de or k.poole@unsw.edu.au

Summary

The skin is equipped with specialized mechanoreceptors that allow the perception of the slightest brush. Indeed some mechanoreceptors can detect even nanometer-scale movements. Movement is transformed into electrical signals via the gating of mechanically-activated ion channels at sensory endings in the skin. The sensitivity of Piezo mechanically-gated ion channels are controlled by stomatin-like protein-3 (STOML3), which is required for normal mechanoreceptor function. Here we identify small molecule inhibitors of STOML3 oligomerization that reversibly reduce the sensitivity of mechanically-gated currents in sensory neurons and silence mechanoreceptors *in vivo*. STOML3 inhibitors in the skin also reversibly attenuate fine touch perception in normal mice. Under pathophysiological conditions following nerve injury or diabetic neuropathy the slightest touch can produce pain, and here STOML3 inhibitors can reverse mechanical hypersensitivity. Thus, small molecules applied locally to the skin can be used to modulate touch and may represent peripherally available drugs to treat tactile-driven pain following neuropathy.

Introduction

All skin sensation starts with the transformation of a physical stimulus into an electrical signal called a receptor potential. The receptor potential is encoded as action potentials (AP), which convey information to the brain to initiate perception[1]. Currently pharmacological agents that modulate the first step in the transformation of light touch stimuli into an electrical signal, a process called sensory mechanotransduction, are not available. The mechanosensitive ion channel Piezo2 and its modulator STOML3[2] have both been shown to be necessary for mechanoreceptors to transduce light touch[3–6]. Paradoxically, under pathophysiological conditions, intense pain can also be triggered by light touch[7,8], for example after traumatic nerve injury[9]. Nerve injury induced touch-evoked pain was found to be largely absent in *Stoml3*$^{-/-}$ mutant mice[6]. STOML3 is an endogenous regulator of the sensitivity of mechanosensitive ion channels like Piezo in sensory neurons and STOML3 self-association appears to be necessary for this function[10,11]. Interestingly, Piezo2 has an essential role in human proprioception and touch sensation[12,13]. Therefore we set out to discover and test whether small molecules that can disrupt STOML3 self-association can be used to modulate touch under normal and pathophysiological conditions.

Identification of small molecule STOML3 inhibitors

In mammals STOML3 belongs to a family of five structurally conserved membrane proteins, including Stomatin, STOML1, STOML2, and Podocin[10,14–18], all of which self-associate via their stomatin-domain (Supplementary Fig. S1a)[10]. Self-association of stomatin-domain proteins can be monitored in HEK293 cells using Bimolecular Fluorescence Complementation (BiFC) whereby N- and C-terminal halves of the YFP molecule are tagged to the prey and bait protein STOML3[2,19] (Fig. 1a). Irreversible association of the YFP fragments produces fluorescence that increases linearly over time (Fig. 1 b). Mutations in one STOML3 pair that disrupt oligomerization (V190P or LR89,90EE) significantly reduce the

rate of signal development (Fig. 1b)[2,10]. We used this cellular assay in a high throughput format to screen for small molecules that significantly inhibit the BiFC signal, a measure of STOML3 self-association. In a primary screen of about 35000 small molecules (each at 20 μM), obtained from the central compound collection of the Leibniz Institute for Molecular Pharmacology screening unit (www.chembionet.info), 21 molecules were found to reproducibly decrease STOML3 self-association based on the slope of YFP signal development. Of these 21 molecules 19 did not pass stringent control tests (see Materials and Methods). The two remaining inhibitory compounds were designated Oligomerization Blocker 1 and 2, (OB-1 and OB-2) (Fig. 1d,e). In further BiFC assays, the STOML3 oligomerization blocker, OB-1 was an effective inhibitor of the self-association of Stomatin, STOML1, STOML2, but not Podocin (Supplementary Fig. 1a). Lower OB-1 concentrations (2 μM) also inhibited the BiFC signal (Supplementary Fig. 1b). The OB-1 molecule was also re-synthesized in house and exhibited the same activity in the BiFC assay as the commercially available sample. The human STOML3 peptide sequence is 92% identical to that of the mouse and 100% identical in the core stomatin-domain and human STOML3 also showed self-association (Fig. 1f). More importantly for potential future clinical development self-association of the human STOML3 protein was also inhibited by OB-1 (Fig 1f).

STOML3 oligomerization dictates domain size in the plasma membrane

We next asked if OB-1 and OB-2 modulation of STOML3 oligomerization state influences clustering of the protein in the plasma membrane. We used super-resolution *d*STORM microscopy[20–22] to visualize FLAG–tagged STOML3 at the plasma membrane of transfected N2a cells. Using *d*STORM we could show that STOML3 was present in microdomains at the plasma membrane (Fig. 1g). The size of the STOML3 clusters was variable (full width at half maximum, FWHM = 24.6 ± 2.8 nm, mean ± sem, Fig. 1h.) but these domains may contain more than one STOML3 dimer[10]. Introduction of the V190P mutation disrupts

oligomerization of STOML3 and abolishes its ability to modulate the mechanosensitivity of Piezo1 channels[2]. This STOML3 variant exhibited significantly smaller clusters in the plasma membrane (Fig. 1g,h), demonstrating that by disrupting STOML3 oligomerization we can manipulate and measure nanoscale changes in STOML3 cluster size. Pre-incubation of N2a cells expressing STOML3-FLAG with OB-1 or OB-2 for three hours led to significantly reduced STOML3-FLAG cluster sizes compared to vehicle treated cells (Fig. 1g,h). The effects of OB-1 did not produce changes in *Stoml3* mRNA levels in these cells (Supplementary Fig. 2a). Thus we obtained independent support for the notion that OB-1 and OB-2 reduce STOML3 oligomerization state, an important consequence of which is a reduced STOML3 cluster size at the plasma membrane.

STOML3 inhibitors modulate mechanotransduction currents

Endogenously expressed STOML3 in N2a cells is required to maintain Piezo channel sensitivity to membrane deflection[2]. By precisely deflecting defined areas of the membrane-substrate interface using a pillar array we could activate Piezo1 currents in N2a cells with displacements ranging from 100 - 1000 nm (Fig. 2a,b). Both OB-1 and OB-2 reduced the sensitivity of mechanosensitive currents to pillar deflection (Fig. 2b). Pre-incubation of cells with OB-1 for periods of between 1 and 3 h reduced Piezo1 current amplitudes, but the effect was only maximal after 3 h (Supplementary Fig. 2b). Recording mechanically-activated currents in the presence of different concentrations of OB-1 revealed a steep concentration dependence with a calculated IC_{50} of 10 nM, Hill coefficient 0.6 (Fig. 2c).

Next we evaluated the effects of OB-1 and OB-2 on mechanosensitive currents in acutely cultured mouse sensory neurons. Neurons were classified on the basis of their AP configuration as mechanoreceptors or nociceptors[2,23]. We found that mechanically gated currents in mechanoreceptors start to activate with membrane deflections of < 50 nm^2, but this sensitivity was substantially reduced after exposure to OB-1 or OB-2 (Fig. 2 d,e). Thus

significant mechanically gated currents were only observed in OB-1 or OB-2 treated cells with deflections that exceeded 100 nm. The threshold for activation of mechanosensitive currents in nociceptive sensory neurons is normally higher than that of mechanoreceptors[2] a finding reproduced here (Fig. 2e,f). However, we also observed that OB-1 or OB-2 treatment produced a significant reduction in the amplitude of mechanically gated currents in nociceptors with stimulus magnitudes between 100 and 500 nm (Fig. 2f). In addition the latency for mechanically gated currents as well as the activation time constant for current activation τ_1 was significantly slowed in nociceptors after treatment with OB-2 (Supplementary Fig. 2 c,d). The exposure of N2a cells or sensory neurons to OB-1 for 3h did not lead to any changes in the level of *Stoml3* transcripts (Supplementary Fig. 2a), suggesting that our molecules change gene expression, or transcript stability. Cell soma indentation can also be used to evoke so called Rapidly-adapting currents (RA-currents, inactivation constant $\tau_2 < 5$ ms) in mechanoreceptor sensory neurons[23,24] and after exposure to OB-1 ~ 60% of the neurons (12/21 neurons) displayed no mechanosensitive current compared to control or vehicle treated neurons (21%, 8/38 neurons), this effect was statistically significant (Fisher's exact test $p < 0.01$ Supplementary Fig. 3a-e). Neither of the two compounds tested had any discernable effects on voltage-gated currents or membrane excitability as evidenced by the fact that APs were of normal amplitude and shape after treatment (Fig. 2h,i). For example, cultured sensory neurons treated for at least 3 h with 20 μM OB-1 displayed no alteration in a number of parameters indicative of electrical excitability (Fig 2g-i, Supplementary Table 1). In summary, using two independent assays we found that OB-1 is a powerful inhibitor of native mechanosensitive currents. Stomatin-domain proteins can also negatively regulate members of the acid sensing ion channel family (ASICs) in a subunit-specific manner [6,10,25,26]. However, OB-1 had no detectable effect on the negative modulation of ASIC3 mediated currents by mouse Stomatin (Supplementary Fig. 4).

A STOML3 inhibitor can silence touch receptors

Many cutaneous mechanoreceptors in *Stoml3*$^{-/-}$ mice innervate the skin, but cannot be activated by mechanical stimulation[5,6]. We made subcutaneous injections of the OB-1 compound (250 - 500 pmol per paw) into the mouse hairy skin innervated by the saphenous nerve and recorded from sensory afferents 3 h later using an *ex vivo* skin - nerve preparation[5,27]. In wild type mice the vast majority of myelinated and unmyelinated fibers are mechanosensitive[4–6], demonstrated by tracing the spike evoked by local electrical stimulation of nerve branches and then searching for the nearby mechanosensitive receptive field (Fig. 3a). In contrast, in skin pre-treated with OB-1 over 39% of Aβ-fibers (19/44) lacked a mechanosensitive receptive field, and this was significantly different from vehicle-injected controls where less than 7% (5/69 fibers) were found to be insensitive to mechanical stimuli, $p < 0.001$ Fischer's exact test (Fig. 3a, Supplementary Table 2). An almost identical proportion of OB-1 treated Aβ-fibers were insensitive to mechanical stimuli in female mice as in male mice (Fig. 3a). Amongst the Aδ-fibers we also observed an increase in the proportion of fibers for which no mechanosensitive receptive field could be found (21%, 8/38 fibers compared to 6%, 1/19 fibers in controls, but this was not significantly different; Fischer's exact test, $p > 0.24$). There was also no change in the proportion of C-fibers that lack a mechanosensitive receptive field (Fig. 3a). We next examined the physiological properties of the remaining mechanosensitive afferents in OB-1 treated skin. However, the proportion of mechanoreceptor types found, as well as the mechanosensitivity of the remaining Aβ-fiber mechanoreceptors (Rapidly and Slowly adapting mechanoreceptors, RAMs and SAMs) was unchanged compared to controls (Supplementary Fig. 5a-e). The mechanoreceptor silencing effect of local OB-1 treatment was completely reversible as recordings from afferents 24 h after treatment revealed no significant loss of mechanosensitivity, also compared to vehicle treated skin (Fig. 3a). Thus, a STOML3

oligomerization inhibitor can specifically and reversibly silence touch receptor activity without changing axonal excitability.

Although, we found no evidence that C-fiber nociceptors are silenced by OB-1 treatment (Fig. 3a) we did note a statistically significant effect of local OB-1 treatment on the mechanosensitivity of C-fiber afferents that respond to both thermal and mechanical stimuli (C-mechanoheat fibers, C-MH, Two-way ANOVA, $p < 0.05$) (Fig. 3b). C-mechanoheat fibers also displayed significantly elevated mechanical thresholds for activation that were on average almost twice that of control fibers (196.5 ± 35.6 mN, mean ± sem in OB-1 treated skin *vs* 106.9 ± 17.4 mN, mean ± sem in vehicle treated skin, Mann-Whitney *U* test, $p < 0.05$) as measured using a force measurement system attached to the stimulus probe (Fig. 3c). The firing rates of C-mechanonociceptors (C-Ms) that lack heat sensitivity, to suprathreshold mechanical stimuli were not significantly attenuated in OB-1 treated skin (Fig. 3d,e).

Touch perception is attenuated by local OB-1 treatment

We used a tactile perception task in head-restrained mice to assess the effects of OB-1 on touch sensation. Water-restricted mice were trained to press a sensor with their forepaw within 500 ms after the onset of a 30 ms cosine mechanical stimulus applied to the same paw. Correct responses were rewarded with water. Mice learned this task to a high degree of reliability after a 7-10 day training period (Fig. 4a). Different stimulus amplitudes were then used to determine a psychometric curve for each mouse (Fig. 4a,b). We next injected the drug vehicle solution into the forepaw and obtained a new psychometric curve for each mouse 3 - 5 h later. On the next day, the forepaw was injected with the OB-1 compound (11 nmol per paw) followed by behavioral testing. At least 24 h after the OB-1 testing day, the recovery behavior was tested without any prior injection. Following OB-1 treatment the psychometric curve was shifted to the right for stimulus strengths between 125-275 μm indicating less reliable stimulus detection (Wilcoxon Signed Rank Test, vehicle *vs* OB-1, $p = 0.026$; OB-1 *vs*

recovery, p = 0.0043) (Fig. 4 b,c). Vehicle treatment produced no significant change in the psychometric curve (Wilcoxon Signed Rank Test, control *vs* vehicle p = 0.30). The detection rates of threshold stimuli returned to pre-treatment levels 1-4 d after treatment (Wilcoxon Signed Rank Test, vehicle *vs* recovery, p = 0.12). These data indicate that silencing of a subset of mechanoreceptors via STOML3 inhibition is sufficient to reduce the reliability of near threshold touch perception in mice.

Peripheral STOML3 blockade reverses tactile allodynia

Neuropathic pain is a debilitating condition in which intense pain can be initiated by merely brushing the skin, activating low-threshold mechanoreceptors[7–9,28,29]. We used the chronic constriction injury model (CCI), which involves direct damage to sciatic nerve axons (Supplementary Fig. 6a-f) that innervate the hypersensitive plantar hindpaw skin. Baseline paw withdrawal thresholds in wild type and *Stoml3*$^{-/-}$ mice did not differ, as measured with von Frey hairs using an adapted up-down method[30] (Fig. 5a). However, after induction of a unilateral CCI[9], paw withdrawal thresholds dropped profoundly in wild type mice but were only moderately reduced in *Stoml3*$^{-/-}$ mice, Two-way ANOVA, $p < 0.001$ (Fig. 5a). Thermal hyperalgesia also accompanies neuropathic injury[7,9,31], a phenomenon that we also observed. However, the heat hyperalgesia observed in *Stoml3*$^{-/-}$ mice was identical to that in wild type controls (Fig. 5b).

We next asked whether local application of OB-1 can ameliorate tactile-evoked pain behavior in neuropathic models. We found no change in paw withdrawal thresholds to mechanical stimuli in the paws of naïve mice treated with an intraplantar dose of OB-1 (250 - 500 pmol per paw) (Fig. 5c). However, when we applied an intraplantar dose of OB-1 to the paws of wild type mice with established neuropathic pain (CCI model 6 - 21 days after induction) we observed a complete reversal of the tactile-evoked pain or allodynia, 0.15 ± 0.06 g (CCI) *vs* 0.7125 ± 0.12 g (OB-1 treated p = 0.0028; paired t-test (Fig. 5d). The effects of OB1 were

also indistinguishable on female and male mice with CCI (Fig 5d)[32]. We also applied OB-1 to the contralateral paw at the same concentration that was effective at reversing allodynia present in the paw ipsilateral to the injury, but observed no reversal of established hypersensitivity (Fig 5e). These results suggest that the actions of OB-1 in reversing hypersensitivity are due to inhibition of sensory neuron mechanotransduction in the skin and not to systemic or central actions. The reversal of tactile allodynia observed with local OB-1 treatment was indistinguishable from that found with systemic gabapentin treatment (Fig. 5f), a standard, centrally acting drug, in clinical use for the treatment of neuropathic pain [33]. Using a series of OB-1 concentrations we could determine a half-maximal effective dose (ED_{50}) of 4.42 μM (or approximately 20 pmol per paw) (Fig. 5g). The effects of a single OB-1 dose became maximal 3 h after the injections and wore off slowly over the next 12 h so that the effect was absent after 24 h (Fig. 5h). To test the idea that OB-1 reverses mechanical hypersensitivity primarily by inhibiting STOML3 oligomerization we tested the effects of local OB-1 on the mechanical sensitivity of *Stoml3*$^{-/-}$ mice with CCI. Mechanical hypersensitivity following CCI is much less prominent in *Stoml3*$^{-/-}$ mice (Fig. 5a,i) but we observed no change in paw withdrawal threshold after treatment of neuropathic paws of *Stoml3*$^{-/-}$ mice with OB-1 (Fig. 5i). Off-target effects are an issue for any biologically active small molecule. We therefore tested the effects of 20μM OB-1 in a commercially available *in vitro* pharmacology panel (www.cerep.fr) consisting of 79 receptors and ion channels (see Supplementary Dataset 1). Significant inhibition of specific ligand binding to the selected receptors was seen in a few cases (6/79), but there is at present no data implicating any of these receptors in peripheral nociception. The agreement between the *in vitro* and *in vivo* effects of STOML3 inhibition and the results of genetic ablation of the *Stoml3* in the mouse suggest that OB-1 exerts its biological effects primarily on STOML3. The remarkable protection from touch-evoked pain in animals lacking STOML3 led us to hypothesize that the

nerve injury may itself lead to a change in the levels of *Stoml3* mRNA expression in the DRG. Up-regulation of STOML3 could in turn exacerbate touch-evoked pain by enhancing the sensitivity of mechanotransduction in injured sensory afferents. Using real-time quantitative PCR we measured a doubling in *Stoml3* mRNA expression levels in the lumbar DRGs that project axons to the ligation site compared to the control uninjured side ($p<0.01$; Mann-Whitney U-test) (Fig. 5j).

The CCI model involves direct damage to the axons that innervate the hypersensitive skin, in this case the plantar hindpaw[34]. Neuropathic touch hypersensitivity is also induced in the same skin area by cutting adjacent nerves to the tibial nerve that innervates the plantar foot [35,36]. Spared tibial nerve injury (SNI) mice develop a long lasting hypersensitivity of similar magnitude to that observed following CCI (Supplementary Fig. 7a). Administration of OB-1 to the plantar skin in the SNI model produced no reversal of allodynia (Supplementary Figure 7b). We removed the lumbar DRGs from these animals and found no change in the levels of *Stoml3* mRNA between the injured and uninjured side in this model (Supplementary Fig.7c). This finding suggests that the effects of OB-1 in alleviating mechanical hypersensitivity may in part depend on whether STOML3 levels are up-regulated.

Mechanical hyperalgesia is also a prominent feature in inflammatory pain, which is largely dependent on increased nerve growth factor (NGF) levels[37]. Systemic dosing with NGF (1 mg/kg) is sufficient to provoke long-lasting mechanical and heat hyperalgesia[37,38], which were both unchanged in NGF-injected *Stoml3*$^{-/-}$ mice (Supplementary Fig. 7d,e). Additionally, mechanical hypersensitivity after NGF was also not reversed by local intraplantar OB-1 (Supplementary Fig. 7f,g). This data is consistent with the prevailing view that NGF-dependent cutaneous mechanical hyperalgesia is primarily driven by central sensitization[37,39].

Regulation of *Stoml3* mRNA and protein after injury

The levels of *Stoml3* mRNA are very low in the DRG and we have never found an antibody that is sensitive or specific enough to detect endogenous STOML3. We therefore generated two new knock-in mouse models to monitor in the first case *Stoml3* gene expression and in the second case STOML3 protein. We created a knockin allele in which a β-galactosidase cassette with a nuclear localization signal (NLS) was fused in frame with the start codon of the *Stoml3* gene (*Stoml3*^{lacZ} mice) (Supplementary Fig. 8 a-c). This reporter allele allowed us to visualize subsets of sensory neurons that express *Stoml3* (Fig. 6a). We observed lacZ staining in around half of sensory neurons with cell bodies > 20 μm in diameter, a population known to consist of mechanoreceptors (Fig. 6a). The number of lacZ-positive neurons more than doubled in the L6-L4 ganglia after a unilateral CCI challenge and the cells were predominantly > 20 μm in diameter, Fisher's exact test, $p < 0.0001$ (Fig. 6b). This data is consistent with the idea that chronic nerve constriction leads to an increase in the number of large and medium sized sensory neurons that express higher levels of *Stoml3*. Consistent with our observation that *Stoml3* mRNA levels are very low in the DRG, the LacZ-positive cells were difficult to visualize when screening for β-galactosidase activity and antibodies directed against the β-galactosidase protein did not give staining. It was therefore difficult to obtain a neurochemical profile of *Stoml3* expressing sensory neurons.

In the second knock-in mouse we introduced nucleotides encoding the StrepII tag[40] 3' to the start codon (Fig 6c, Supplementary Fig. 8d-f). The genomic fusion was successful as we could amplify *Stoml3* mRNA transcripts containing the nucleotide sequence encoding an N-terminally StrepII-tagged *Stoml3*. We carried out Western blotting for the StrepII-tagged protein in *Stoml3*^{StrepII} CCI mice and extracted protein from sciatic nerve at day 2, day 6 and day 13 post-injury. We could detect a specific band (absent in *Stoml3*$^{-/-}$ nerve) of the appropriate molecular weight in protein extracts from the sciatic nerve, but only after using a strong denaturing buffer containing 8M urea (Fig 6d). We could sometimes detect the

StrepII-STOML3 band from extracts made from DRG but this was much weaker and less reliable (data not shown). Notably, we found more intense -STOML3-StrepII positive bands on the injured side at day 2, day 6 and to a lesser extent at day 13 compared to the non-injured contralateral nerve (Fig. 6d). The fact that the neuronal marker PGP9.5 band, dramatically decreased in intensity on the injured side several days after injury, probably reflects axon loss and atrophy, despite this STOML3 levels were increased. These results suggest that endogenous STOML3 is transported preferentially to the peripheral endings of sensory neurons[41] to modulate mechanotransduction and that there is more STOML3 transported to sensory endings after traumatic nerve injury.

STOML3 and painful diabetic neuropathy

Neuropathy is a prominent symptom of diabetes, and is often characterized by pain initiated by normally innocuous tactile stimulation in up to 20% of all patients[42]. We next asked whether OB-1 shows efficacy in a mouse model of painful diabetic neuropathy. We used the streptozotocin model (STZ) to induce mechanical hypersensitivity in mice with diabetes[43]. Between 6-7 weeks after STZ treatment, mice assigned to the drug and vehicle group began to display hypersensitivity to mechanical stimuli as reflected in increased frequency of paw withdrawal to von Frey filaments below 0.5 g (Fig. 7 a-d). Local treatment of the hindpaw glabrous skin with OB-1 (250 pmol per paw) substantially reversed the mechanical hypersensitivity 4 h after treatment whereas vehicle treatment was without effect (Fig 7a-d), PWT = 0.93 ± 0.13 g (OB-1 treated) *vs* 0.32 ± 0.06 (STZ), paired t-test, p = 0.0013 (Fig. 7b) or PWT = 0.63± 0.13 g (vehicle treated) *vs* 0.51± 0.01 (STZ), paired t-test, p = 0.31 (Fig. 7d). The mechanical hypersensitivity returned to pre-drug treatment levels 24 h after a single treatment, as assessed by the mean 60% withdrawal threshold (Fig. 7a,b).

Discussion

Mammalian touch sensation is at last beginning to be unraveled at the molecular level[44,45]. Mechanosensitive ion channels, like Piezo1 and Piezo2, may prove difficult targets to exploit for pharmacological intervention[46]. For example, the early embryonic or post-natal lethality associated with *Piezo1* or *Piezo2* gene deletion[47,48] and Piezo2's role in proprioception[12,13,49] could prove problematic for the development of Piezo antagonists for therapeutic purposes. Here we describe an intersectional approach to modulate sensory mechanotransduction as our compounds should only be effective in cells in which both STOML3 and Piezo channels are present. This approach has the advantage that essential functions of Piezo proteins will not be directly affected by our small molecules yet we can gain selective and powerful inhibition of sensory mechanotransduction, especially under some pathophysiological conditions. We show that OB-1 has a powerful silencing effect on around 40% of mechanoreceptors and conclude that the transformation of the mechanical stimulus into receptor potential is severely impaired in these cells. Mechanosensitive currents were also inhibited by OB-1 in some nociceptors in our in vitro studies (Fig. 2f) and consistent with this mechanical thresholds were significantly elevated in many cutaneous C-fibers measured using the *ex vivo* skin-nerve preparation (Fig. 3). We propose that STOML3 inhibition silences mechanoreceptors primarily by reducing the displacement sensitivity of Piezo2 ion channels in mechanoreceptors. Mechanically gated currents in nociceptors may not be dependent on Piezo2[4], but deep sequencing studies have detected Piezo1 transcripts in many single mouse sensory neurons[50] and Piezo1 channels are also strongly modulated by STOML3[2]. Skin application of our STOML3 inhibitor OB-1 shows remarkable efficacy in reducing touch-evoked pain behavior in two mouse models of neuropathic pain, but not in an SNI model. There is direct damage to the axons that innervate the sensitized skin in the CCI model that is associated with increased *Stoml3* expression as well as increased STOML3 protein transport

to the periphery (Fig. 6). Thus, we speculate that the remarkable efficacy of OB-1 in some pain models, including painful diabetic neuropathy is directly linked to changes in STOML3 availability at sensory endings during disease progression. Stoml3 mRNA transcript expression has been detected in human tibial nerve and skin (http://gtexportal.org) and so it may be possible to detect changes in STOML3 in pathologies associated with neuropathic pain. In summary, we provide mechanistic validation of a novel pharmacological strategy to modulate sensory mechanotransduction to treat sensory disorders including pain.

Accession Codes

N/A

Data Availability Statement

All materials and datasets are available on request

Acknowledgements

We thank Kathleen Barda, Maria Braunschweig, and Heike Thraenhardt for technical assistance and Gregor Lichtner for providing the custom written algorithm for *d*STORM drift correction. We also thank Bettina Purfürst for electron microscopy experiments. This study was funded by a DFG collaborative research grant SFB958 (projects A09 to K.P and G.R.L., A01 to V.H. and Z02 to J.S.). Additional support was provided by a senior ERC grant (Grant number 294678 to G.R.L) and the Neurocure excellence cluster (to V.H., G.R.L., and J.F.A.P.). K.P was supported by a Cecile-Vogt Fellowship (MDC). S.P. was supported by Marie Curie fellowship from the European Union (Grant number 253663 Touch in situ). C.P. received a Ph.D fellowship from the University of Cagliari. J.F.A.P. was funded by a European Research council (ERC) starting grant (ERC-2010-StG-260590), the DFG (FOR 1341, FOR 2143), the Berlin Institute of Health (BIH) and the European Union (FP7, 3x3Dimaging 323945). RK was supported by an ERC Advanced Investigator grant (294293 - PAIN PLASTICITY). DH was funded by the Berlin Institute of Health (BIH). EStJ Smith, LE and MM were supported by an Alexander von Humboldt fellowship. We would like to thank H.Wende for providing help and advice for generating the Stoml3^{lacZ} allele and S. Lechner for comments on the MS.

Author Contributions

KP designed and carried out the screen, and characterized small molecules with *d*STORM and patch clamp electrophysiology. CW performed ex vivo skin electrophysiology and

experiments in mice and behavioral experiments. SP screened OB-1 for effects on mechanosensitive currents in DRGs. CP performed behavioral and real time PCR experiments and performed histochemical analysis of the *Stoml3*^{lacz} mice. CG determined IC50s using the pili method. DH performed touch perception assays with LE who established the methodology. KKB established the diabetic neuropathay model and performed behavioral experiments. AL performed and analyzed *d*STORM experiments with LL, VB, KP, CP and JW generated and characterized the *Stoml3*^{lacz} and *Stoml*^{StrepII} mice. LL and RF performed molecular cloning experiments. Est.JS performed ASIC experiments. MM performed additional electrophysiological experiments. JK analysed transmission electron microscopy data. ES synthesized molecules and managed compound libraries. MN performed statistical analyses of high throughput screening data and helped in design and execution of the screen. JPvK supervised screening experiments. JFAP established touch perception assays and supervised the acquisition and analysis of the data. VH and JS directed and supervised imaging experiments. KP, CW and GRL wrote the paper. KP, CW and GRL conceived and directed the project.

Competing Financial Interests Statement

G.R.L., K.P.,C.W., E.S., L.L. are named as inventors on a patent application related to data in this paper.

References

1. Bensmaia, S. J. Tactile intensity and population codes. *Behav*. *Brain Res*. **190,** 165–173 (2008).
2. Poole, K., Herget, R., Lapatsina, L., Ngo, H.-D. & Lewin, G. R. Tuning Piezo ion channels to detect molecular-scale movements relevant for fine touch. *Nat*. *Commun*. **5,** 3520 (2014).
3. Woo, S.-H. *et al*. Piezo2 is required for Merkel-cell mechanotransduction. *Nature* (2014). doi:10.1038/nature13251
4. Ranade, S. S. *et al*. Piezo2 is the major transducer of mechanical forces for touch sensation in mice. *Nature* **516,** 121–125 (2014).
5. Moshourab, R. A., Wetzel, C., Martinez-Salgado, C. & Lewin, G. R. Stomatin-domain protein interactions with acid-sensing ion channels modulate nociceptor mechanosensitivity. *J*. *Physiol*. **591,** 5555–5574 (2013).
6. Wetzel, C. *et al*. A stomatin-domain protein essential for touch sensation in the mouse. *Nature* **445,** 206–209 (2007).

7. Costigan, M., Scholz, J. & Woolf, C. J. Neuropathic pain: a maladaptive response of the nervous system to damage. *Annu. Rev. Neurosci.* **32,** 1–32 (2009).
8. von Hehn, C. A., Baron, R. & Woolf, C. J. Deconstructing the Neuropathic Pain Phenotype to Reveal Neural Mechanisms. *Neuron* **73,** 638–652 (2012).
9. Tal, M. & Bennett, G. J. Extra-territorial pain in rats with a peripheral mononeuropathy: mechano-hyperalgesia and mechano-allodynia in the territory of an uninjured nerve. *Pain* **57,** 375–382 (1994).
10. Brand, J. *et al*. A stomatin dimer modulates the activity of acid-sensing ion channels. *EMBO J.* **31,** 3635–3646 (2012).
11. Poole, K. *et al*. Tuning Piezo ion channels to detect molecular-scale movements relevant for fine touch. *Nat. Commun.* **5,** 3520 (2014).
12. Chesler, A. T. *et al*. The Role of *PIEZO2* in Human Mechanosensation. *N. Engl. J. Med.* **375,** 1355–1364 (2016).
13. Mahmud, A. A. *et al*. Loss of the proprioception and touch sensation channel PIEZO2 in siblings with a progressive form of contractures. *Clin. Genet*. (2016). doi:10.1111/cge.12850
14. Wang, Y. & Morrow, J. S. Identification and characterization of human SLP-2, a novel homologue of stomatin (band 7.2b) present in erythrocytes and other tissues. *J. Biol. Chem.* **275,** 8062–8071 (2000).
15. Boute, N. *et al*. NPHS2, encoding the glomerular protein podocin, is mutated in autosomal recessive steroid-resistant nephrotic syndrome. *Nat. Genet.* **24,** 349–354 (2000).
16. Mairhofer, M., Steiner, M., Salzer, U. & Prohaska, R. Stomatin-like protein-1 interacts with stomatin and is targeted to late endosomes. *J. Biol. Chem.* **284,** 29218–29229 (2009).
17. Da Cruz, S. *et al*. SLP-2 interacts with prohibitins in the mitochondrial inner membrane and contributes to their stability. *Biochim. Biophys. Acta* **1783,** 904–911 (2008).
18. Lapatsina, L., Brand, J., Poole, K., Daumke, O. & Lewin, G. R. Stomatin-domain proteins. *Eur. J. Cell Biol.* **91,** 240–245 (2012).
19. Hu, C.-D., Chinenov, Y. & Kerppola, T. K. Visualization of interactions among bZIP and Rel family proteins in living cells using bimolecular fluorescence complementation. *Mol. Cell* **9,** 789–798 (2002).
20. Heilemann, M. *et al*. Subdiffraction-resolution fluorescence imaging with conventional

fluorescent probes. *Angew*. *Chem*. *Int*. *Ed*. *Engl*. **47,** 6172–6176 (2008).
21. Lampe, A., Haucke, V., Sigrist, S. J., Heilemann, M. & Schmoranzer, J. Multi-colour direct STORM with red emitting carbocyanines. *Biol*. *Cell* **104,** 229–237 (2012).
22. Wolter, S. *et al*. rapidSTORM: accurate, fast open-source software for localization microscopy. *Nat*. *Methods* **9,** 1040–1041 (2012).
23. Hu, J. & Lewin, G. R. Mechanosensitive currents in the neurites of cultured mouse sensory neurones. *J*. *Physiol*. **577,** 815–828 (2006).
24. McCarter, G. C., Reichling, D. B. & Levine, J. D. Mechanical transduction by rat dorsal root ganglion neurons in vitro. *Neurosci*. *Lett*. **273,** 179–182 (1999).
25. Price, M. P., Thompson, R. J., Eshcol, J. O., Wemmie, J. A. & Benson, C. J. Stomatin modulates gating of acid-sensing ion channels. *J*. *Biol*. *Chem*. **279,** 53886–53891 (2004).
26. Kozlenkov, A., Lapatsina, L., Lewin, G. R. & Smith, E. S. J. Subunit-specific inhibition of acid sensing ion channels by stomatin-like protein 1. *J*. *Physiol*. **592,** 557–569 (2014).
27. Milenkovic, N., Wetzel, C., Moshourab, R. & Lewin, G. R. Speed and temperature dependences of mechanotransduction in afferent fibers recorded from the mouse saphenous nerve. *J*. *Neurophysiol*. **100,** 2771–2783 (2008).
28. Lewin, G. R. & Moshourab, R. Mechanosensation and pain. *J*. *Neurobiol*. **61,** 30–44 (2004).
29. Beggs, S., Trang, T. & Salter, M. W. P2X4R+ microglia drive neuropathic pain. *Nat*. *Neurosci*. **15,** 1068–1073 (2012).
30. Chaplan, S. R., Bach, F. W., Pogrel, J. W., Chung, J. M. & Yaksh, T. L. Quantitative assessment of tactile allodynia in the rat paw. *J*. *Neurosci*. *Methods* **53,** 55–63 (1994).
31. Baron, R. Neuropathic pain: a clinical perspective. *Handb*. *Exp*. *Pharmacol*. 3–30 (2009). doi:10.1007/978-3-540-79090-7_1
32. Sorge, R. E. *et al*. Different immune cells mediate mechanical pain hypersensitivity in male and female mice. *Nat*. *Neurosci*. **18,** 1081–1083 (2015).
33. Dworkin, R. H. *et al*. Recommendations for the pharmacological management of neuropathic pain: an overview and literature update. *Mayo Clin*. *Proc*. **85,** S3-14 (2010).
34. Basbaum, A. I., Gautron, M., Jazat, F., Mayes, M. & Guilbaud, G. The spectrum of fiber loss in a model of neuropathic pain in the rat: an electron microscopic study. *Pain* **47,** 359–67 (1991).

35. Decosterd, I. & Woolf, C. J. Spared nerve injury: an animal model of persistent peripheral neuropathic pain. *Pain* **87,** 149–158 (2000).
36. Shields, S. D., Eckert, W. A. & Basbaum, A. I. Spared nerve injury model of neuropathic pain in the mouse: a behavioral and anatomic analysis. *J. Pain Off. J. Am. Pain Soc.* **4,** 465–470 (2003).
37. Lewin, G. R., Lechner, S. G. & Smith, E. S. J. Nerve growth factor and nociception: from experimental embryology to new analgesic therapy. *Handb. Exp. Pharmacol.* **220,** 251–282 (2014).
38. Lewin, G. R. *et al*. Nerve growth factor-induced hyperalgesia in the neonatal and adult rat. *J. Neurosci.* **13,** 2136–48 (1993).
39. Lewin, G. R., Rueff, A. & Mendell, L. M. Peripheral and central mechanisms of NGF-induced hyperalgesia. *Eur. J. Neurosci.* **6,** 1903–12 (1994).
40. Korndörfer, I. P. & Skerra, A. Improved affinity of engineered streptavidin for the Strep-tag II peptide is due to a fixed open conformation of the lid-like loop at the binding site. *Protein Sci.* **11,** 883–93 (2002).
41. Lapatsina, L. *et al*. Regulation of ASIC channels by a stomatin/STOML3 complex located in a mobile vesicle pool in sensory neurons. *Open Biol.* **2,** 120096 (2012).
42. van Hecke, O., Austin, S. K., Khan, R. A., Smith, B. H. & Torrance, N. Neuropathic pain in the general population: a systematic review of epidemiological studies. *Pain* **155,** 654–662 (2014).
43. Bierhaus, A. *et al*. Methylglyoxal modification of Nav1.8 facilitates nociceptive neuron firing and causes hyperalgesia in diabetic neuropathy. *Nat. Med.* **18,** 926–933 (2012).
44. Abraira, V. E. & Ginty, D. D. The sensory neurons of touch. *Neuron* **79,** 618–639 (2013).
45. Lechner, S. G. & Lewin, G. R. Hairy sensation. *Physiology (Bethesda).* **28,** 142–150 (2013).
46. Syeda, R. *et al*. Chemical activation of the mechanotransduction channel Piezo1. *Elife* **4,** (2015).
47. Li, J. *et al*. Piezo1 integration of vascular architecture with physiological force. *Nature* (2014). doi:10.1038/nature13701
48. Ranade, S. S. *et al*. Piezo1, a mechanically activated ion channel, is required for vascular development in mice. *Proc. Natl. Acad. Sci. U. S. A.* **111,** 10347–10352 (2014).

523 49. Woo, S.-H. *et al*. Piezo2 is the principal mechanotransduction channel for
524 proprioception. *Nat*. *Neurosci*. **18,** 1756–62 (2015).
525 50. Usoskin, D. *et al*. Unbiased classification of sensory neuron types by large-scale
526 single-cell RNA sequencing. *Nat*. *Neurosci*. **18,** 145–153 (2015).
527
528

Figure Legends

Figure 1 Screening for small molecules that modulate STOML3 oligomerization. **a**, Schematic representation of BiFC analysis of protein-protein interactions used for small molecule screen. **b**, Signal development observed when STOML3-VC was used as prey and VN-tagged STOML3 variants that do not properly oligomerize were used as bait. **c,** The normalized slope of BiFC signal development was used as a measure of oligomerization. ** $p < 0.01$ *** $p < 0.001$; unpaired t-test, two-tailed with $p = 0.0046$ ($t=3.629$ $df=10$) STOML3 *vs*. STOML3-V190P, $p < 0.0001$ ($t=9.265$ $df=10$) STOML3 *vs*. STOML3LR89,90VP, $p < 0.0001$ ($t=12.15$ $df=10$) STOML3 *vs*. un-transfected cells; numbers indicate replicate TECAN experiments derived from 4-6 independent transfections; data are shown as individual slopes and mean ± s.e.m. **d**, Structures of hit compounds, the oligomerization blockers, OB-1 and OB-2. **e,f**, Normalized slope of BiFC signal development in cells overexpressing Mus musculus or Homo sapiens STOML3 in the presence of OB-1 and OB-2 is shown. ** $p < 0.01$ *** $p < 0.001$; (i) unpaired t-test, two-tailed with $p=0.0002$ ($t=6.594$ $df=8$) mmSTOML3 *vs*. mmSTOML3 + OB-1, $p=0.0064$ ($t=3.527$ $df=9$) mmSTOML3 *vs*. mmSTOML3 + OB-2; numbers indicate replicate TECAN experiments derived from 4-6 independent transfections; data are displayed as individual slopes and mean ± s.e.m.; mean ± s.e.m. (e); (ii) Mann-Whitney *U* test, two tailed with $p = 0.0002$ (Sum of ranks 100 , 36 U 0) hsSTOML3 *vs*. hsSTOML3 + OB-1; numbers indicate replicate TECAN experiments derived from two independent transfections with 4 replicates each; data are shown as individual slopes and mean ± s.e.m. (f). **g**, Representative reconstructed *d*STORM images of STOML3-FLAG overexpressed in N2a cells. **h**, Distribution of STOML3-FLAG domain size as detected by *d*STORM imaging. ** $p < 0.01$ *** $p < 0.001$; unpaired t-test, two-tailed, with $p = 0.0023$ ($t=3.496$ $df=20$) STOML3 *vs*. STOML3-V190P, $p < 0.0001$ ($t=6.533$ $df=26$) STOML3 *vs*. STOML3 + OB-1, $p = 0.0006$ ($t=3.994$ $df=23$) STOML3 *vs*. STOML3 + OB-; numbers indicate N2a cells derived from at least 3 transfections. Each data point represents a single cell, for each cell the FHWM of 100 randomly chosen domains was measured.

Figure 2 Quantitative analysis of the effect of hit compounds on mechanotransduction. **a**, Schematic of pillar array analysis of mechanotransduction in N2a cells. **b**, Stimulus-response curves for N2a treated with either OB-1 or OB-2; both compounds significantly inhibit mechanically-gated currents in N2a cells. ** $p < 0.01$ *** $p < 0.001$; (i) Two-way ANOVA (stimulus response relationship) with $p=0.0044$ $F(1, 131) = 8.390$ Vehicle *vs*. OB-

1, p = 0.0388 F (1, 108) = 4.375 Vehicle *vs*. OB-2, numbers indicate stimulus response curves for N2a cells from > 5 independent experiments, data are displayed as mean of individual bins ± s.e.m.; (ii) Mann- Whitney *U*-test, two-tailed, Bin 250-500 with p=0.0146 (U=27.00) Vehicle *vs*. OB1, p=0.0363 (U=23.50) Vehicle *vs*. OB2; numbers indicate cells stimulated in this range, data are displayed as mean current amplitude of individual bins ± s.e.m.. **c**, Hill plot of the concentration dependence of the OB-1 effect on the Piezo1 current in N2a cells. ** p < 0.05; Mann-Whitney *U* test with p = 0.9266 Vehicle *vs*. 0.002µM OB-1, p = 0.1236 Vehicle *vs*. 0.02µM OB-1, p = 0.1112 Vehicle *vs*. 2µM OB-1, p = 0.0105 Vehicle *vs*. 20µM OB-1; numbers indicate N2a cells recorded in 2 (Vehicle), 4 (0.002µM), 3 (0.2µM), 3 (2µM), 3 (20µM OB1) independent experiments, data are displayed as mean current amplitude of individual bins ± s.e.m.. **d**, Schematic of pillar array analysis of mechanotransduction in acutely prepared DRG neurons. **e**, Stimulus-response curves for mechanoreceptors treated with either OB-1 or OB-2; both compounds significantly inhibit mechanically-gated currents activated by pillar deflections less than 50 nm, OB-1 significantly inhibits currents gated by deflections up to 250 nm. * p < 0.05 ** p < 0.01 *** p < 0.001; (i) Two-way ANOVA with p = 0.0007 (F (1, 80) = 12.56) Vehicle *vs*. OB-1, p = 0.0017 (F (1, 78) = 10.59) Vehicle *vs*. OB-2; numbers indicate recorded stimulus-responses curves of DRG mechanoreceptors from at least 3 DRG preps; (ii) unpaired t-test, two-tailed, Bin 0-10 with p = 0.0462 (t=2.246 df=11) Vehicle *vs*. OB1, p = 0.0291 (t=2.477 df=12) Vehicle *vs*. OB2; (iii) Mann-Whitney *U* test, two tailed, Bin 10-50 with p = 0.0053 Vehicle *vs*. OB-1, p = 0.0068 Vehicle *vs*. OB-2, Bin 50-100 with p = 0.0224 Vehicle *vs*. OB-1, Bin 100-500 with p = 0.0239 Vehicle *vs*. OB-1; numbers indicate currents measured from DRG mechanoreceptors, data from at least 3 DRG cultures derived from 5-7 weeks old mice; data are displayed as current amplitude, each bin displayed as mean of cell averages ± s.e.m.. **f,** Stimulus-response curves for nociceptors treated with either OB-1 significantly inhibit mechanically-gated currents in these cells. * p < 0.05, (i) Two-way ANOVA with p = 0.0263 (F (1, 80) = 12.56) (F (1, 78) = 10.59) Vehicle *vs*. OB-1, *ns* (F (1, 78) = 10.59) Vehicle *vs*. OB-2, numbers indicate stimulus-response curves in DRG nociceptors derived from at least 3 DRG preparations derived from 5-7 weeks old mice ; data are displayed as current amplitude, each bin displayed as mean of cell averages ± s.e.m; (ii) Mann-Whitney *U* test with p =0.0388 (U=10.00, Bin 100-250) Vehicle *vs*. OB-1, p = 0.0087 (U=2.000, Bin 250-500) Vehicle *vs*. OB-2; numbers indicate currents measured in DRG nociceptors, at least 3 DRG preparations derived from 5-7 weeks old mice; data are displayed as current amplitude, each bin displayed as mean of cell averages ± s.e.m.. **g-i,** In the presence of OB-1

there was no detectable difference in action potentials generated by current injection in either (**h**) mechanoreceptors or (**i**) nociceptors, statistical tests applied: (i) Mann-Whitney *U* test (Mechanoreceptors) with p = 0.215 (U=19); (ii) Student's t-test (Nociceptors), two-tailed with p = 0.4743 (F=2.682, DFn=11, Dfd=12); numbers indicate cultivated neurons recorded from 3 mice in 3 independent experiments; data are displayed as current amplitudes and mean of individual bins ± s.e.m..

Figure 3 Mechanoreceptors can be silenced with local OB-1 treatment.

a, Inset: Electrical search protocol schema. A micro electrode (~1MΩ) was used to deliver electrical stimuli at two distant points of the saphenous nerve trunk in order to trace electrically identified units to their receptive fields. Proportions of mechano*IN*sensitive fibers are shown. Three hours after local OB-1 treatment (250 -500 pmol OB-1 per paw) an increase in mechanically *IN*sensitive Aβ-fibers was observed; note that mechanosensitivity had recovered 24h post-injection. ** $p < 0.01$ *** $p < 0.001$; Fisher's exact test with $p < 0.0001$ Aβ-fibers Vehicle *vs*. OB-1(male & female mice), $p < 0.0001$ (Aβ-fibers Vehicle *vs*. OB-1 (male), p = 0.0033 Aβ-fibers Vehicle *vs*. OB-1(female), p = 1.0 (Aβ-fibers OB-1(male) *vs*. OB-1 (female), p = 0.0028 Aβ-fibers OB-1 *vs*. OB-1 wash-out, p = 0.2465 Aδ-fibers Vehicle *vs*. OB-1, p = 1.0 C-fibers Vehicle *vs*. OB-1; numbers indicate single sensory fiber recordings derived from 10-20 independent experiments using adult mice (Fig 3a-e together), data are displayed as percentage of individual fibers. **b,** Stimulus response function of C-MH fibers is shown using a series of ascending displacements (32 – 1024 µm). C-MH fibers were significantly less responsive in OB-1 treated mice compared to vehicle treated controls. * $p < 0.05$; Two-way ANOVA with p = 0.0412 (F=4.208, DFn=1, Dfd=257) Vehicle *vs*. OB-1; numbers indicate fibers recorded in 10-20 independent experiments; data are displayed as mean number of action potentials ± s.e.m.. **c,** Mean force thresholds for C-MH fiber discharge are displayed showing a significant elevation of mechanical thresholds. * $p < 0.05$; Mann-Whitney *U* test with p=0.0233 (U = 89); numbers indicate single sensory fiber recordings derived from 10-20 independent experiments using adult mice (Fig 3a-e together); data are displayed as individual thresholds and mean threshold ± s.e.m.. **d,** For C-M fibers there was no significant difference between vehicle and OB-1 treated stimulus response functions. Statistical test applied: Two-way ANOVA with p = 0.3563 (F=0,8579,DFn=1, Dfd=115); numbers indicate single sensory fiber recordings derived from 10-20 independent experiments using adult mice (Fig 3a-e together); data are displayed as mean number of action potentials ± s.e.m.. **e**, Mean force thresholds for C-M fiber were also not different

between vehicle and OB-1 treatments. Statistical test applied: unpaired t-test, two tailed with p = 0.7860 t=0,2756 df=18;numbers indicate single sensory fiber recordings derived from 10-20 independent experiments using adult mice (Fig 3a-e together); data are displayed as individual thresholds and mean threshold ± s.e.m.).

Figure 4 OB-1 reduces the touch perception in mice

A tactile perception task for head-restrained mice. **a,** Mice were trained to report a single tactile pulse stimulus (inset shows stimulus voltage command pulse for all 8 amplitudes). Trial structure: mice were trained to (1) hold the rest sensor and wait for a stimulus; (2) on detection of the stimulus reach and press the target sensor within 500 ms from stimulus onset; (3) obtain water reward by licking providing it was a successful trial. **b,** Psychometric curves to different amplitude tactile stimuli are affected by injection of OB-1 into forepaw. Curves were constructed with a sigmoid fitting of the mean hit rates to 7 different amplitudes of tactile stimuli and a no stimulus trial (false alarm). Three conditions are displayed, injection of the vehicle (black), injection of OB-1 (magenta) and a recovery session with no prior injection (grey). **c,** OB-1 application to forepaw attenuates perception of near threshold tactile stimuli. Grouped hit rates to 3 threshold amplitude values (125, 175 and 275 μm) from 5 mice were significantly reduced after OB-1 injection as compared to hit rates after vehicle injection or on recovery session without prior injection. Statistical tests were made on hit rates after subtraction of the corresponding false alarm rates. * $p < 0.05$; Wilcoxon Signed Rank Test with p = 0.026 Vehicle *vs*.. OB-1, p = 0.0043 OB-1 *vs*.. OB-1 Wash-out, p = 0.12 Vehicle *vs*.. OB-1 Wash-out; numbers indicate mice treated, data are displayed as average of individual hit rates of each mouse, grouped for 3 amplitudes ± s.e.m..

Figure 5 Tactile-evoked pain can be treated with OB-1.

a, Development of tactile-evoked pain after traumatic nerve injury is shown. Paw withdrawal thresholds (PWT) to varying forces of von Frey filaments before and after unilateral CCI were measured. Note that after nerve injury *Stoml3*$^{-/-}$ mice develop significantly less tactile-evoked pain compared to wild type animals. *** $p < 0.001$ ** $p < 0.01$; Two-way ANOVA with $p < 0.0001$ (F=107,65, DFn=1, Dfd=159) WT *vs*. *Stoml3*$^{-/-}$ and Bonferroni's multiple comparison with p > 0,9999, t = 1,488 df=159 (d0), p = 0,3728, t = 2,056 df = 159 (d2), p = 0.0027, t = 3,701 df = 159 (d4), p = 0.0006, t = 4,104 df = 159 (d6), p = 0.006, t = 4,096 df = 159 (d8), p = 0.003, t = 4,273 df = 159 (d10), p < 0.0001, t =5,255df = 159 (d12), p = 0.0303, t = 2,977 df = 159 (d14), p = 0.0048, t = 3,535 df = 159 (d21); numbers indicate

numbers of adult mice examined from two cohorts tested independently; data are displayed as mean of individual median PWTs ± s.e.m.. **b,** Paw withdrawal latencies (PWLs) to a standard radiant heat source applied to the ipsilateral hind paw of wild type and *Stoml3*$^{-/-}$ mice before and after CCI were not different between the genotypes. ** $p < 0.01$ * $p < 0.05$; Mann-Whitney *U* test with p = 0.0065 WT (U = 1.500) naive *vs*. WT CCI, p = 0.0325 (U = 4.500) *Stoml3*$^{-/-}$ naive *vs*. *Stoml3*$^{-/-}$ CCI, p = 0.2532 (U= 10.50) WT CCI *vs*. Stoml3$^{-/-}$ CCI ; numbers indicate mice treated (one cohort); data are displayed as mean PWL ± s.e.m.). **c**, Treatment of naïve mice with OB-1 does not alter PWTs, paws of mice treated, (12= ipsi and contra; 6=ipsi, 6=contra) one cohort, *ns* Mann-Whitney *U* test with p = 0.2042 (U = 22) Naïve *vs* OB-1 treated, p = 0.4545 (U = 14) OB-1 treated *vs*. Vehicle treated; numbers indicate adult mice treated; data are displayed as mean of individual median PWTs. **d-e**, PWT measured before and after nerve injury shows clear hypersensitivity that is not reversed by injection of vehicle, note that local ipsilateral treatment of the neuropathic paw with OB-1 effectively normalizes PWT, but treatment of the contralateral paw does not (e). ** $p < 0.01$ * $p < 0.05$; (i) paired t-test, two tailed with p = 0.0028 (t=3,570 df=15) CCI male & female *vs*. CCI + OB-1 male & female), p = 0.0066 (t=3,811 df=7) CCI male *vs*. CCI + OB-1 male, p = 0.0193 (t=3,022 df=7) CCI female *vs*. CCI + OB-1 female), (ii) Mann-Whitney *U* test with p= 0.25 (U = 7) CCI ipsi *vs*. OB-1contralateral injected ipsilateral measured; numbers indicate adult mice examined from three cohorts tested independently; data are displayed as mean of individual median PWTs; ± s.e.m.**. f,** Note that alleviation of hypersensitivity with OB-1 treatment is indistinguishable from gabapentin treatment. ** $p < 0.01$; Wilcoxon matched-pairs signed rank test with p = 0.0013 (t=6,518 df=5) CCI *vs*. CCI + Gabapentin; numbers indicate adult mice treated (one cohort tested), data are displayed as mean of individual median PWTs; error bars indicate s.e.m.. **g,** Dose-response relationship of OB-1 is shown, ED_{50} = 4.42 µM or approximately 20 pmol. *** $p < 0.001$ ** $p < 0.01$; Mann-Whitney *U* test with p = 0.7265 Vehicle *vs*. 0.5µM OB-1, p = 0.0749 Vehicle *vs*. 5µM OB-1, p = 0.0002 Vehicle *vs*. 50µM OB-1, p = 0.0044 Vehicle *vs*. 100µM OB-1; numbers indicate drug treatments, adult mice came from 9 cohorts; data are displayed as mean of individual median PWTs; error bars indicate s.e.m.. **h,** Measurement of PWTs over time; the maximal analgesic efficacy developed between 3h and 9h after local OB-1 injection; numbers indicate mice treated (one cohort tested); data are displayed as mean of individual median PWTs. **i,** No significant change in PWT was measured in *Stoml3*$^{-/-}$ mice with CCI after local administration of OB-1, paired t-test with p =0.125 (Sum of signed ranks = 13.00 Number of pairs = 6) CCI, *Stoml3*$^{-/-}$ *vs*. CCI, *Stoml3*$^{-/-}$ + OB-1; numbers indicate drug treatments (one

cohort tested); data are displayed as mean of individual median PWTs; error bars indicate s.e.m.. **j,** S*toml3* copy number derived from lumbar DRG L4-6 determined using real-time PCR showing an ipsilateral up-regulation of *Stoml3* mRNA. Note that the last two bars represent data from *Stoml3*$^{-/-}$ mice. ** $p < 0.01$, * $p < 0.05$; Mann-Whitney *U* test with p=0.0079 (U = 0) CCI ipsi *vs*. contra, p=0.0357 (U = 0) naive ipsi *vs*. CCI ipsi, p=0.7000 (U = 4) naive ipsi *vs*. contra numbers indicate RNA preparations with L4-6 of two adult mice pooled for one RNA preparation; data represent the mean copy number ± s.e.m.).

Figure 6 Regulation of STOML3 in painful neuropathy

a, Cytochemistry of lumbar DRGs from *Stoml3*$^{+/lacZ}$ mice that had received a nerve injury (CCI). **b,** Note that the number of lacZ-positive neurons increased after a unilateral CCI predominantly in large cells.***$p < 0.001$; Fisher's exact test with $p < 0.0001$; numbers indicate cells counted analyzing 23 images obtained from 10 adult *Stoml3*$^{lacZ/lacZ}$ mice or 17 images obtained from adult *Stoml3*$^{+/lacZ}$ mice. **c**, schematic of the modified locus of StrepII knockin mice. **d**, Western blots of protein extracts taken from the sciatic nerve of 2 adult *Stoml3*$^{StrepII/StrepII}$ knockin mice per protein preparation subjected to unilateral CCI. Extracts were made from two mice per time point note that a specific StrepII-STOML3 band was detected ipsiliateral and contralateral to the injury at all time points (bands are not detected in protein extracts from sciatic nerves of 2 adult *Stoml3*$^{-/-}$ mice per protein preparation). At day 2 (d2), day 6 (d6) and to a lesser extent day 13 (d13) post-injury there was clearly much more protein found on the injured side compared to the uninjured sciatic nerve. The same protein extracts were probed with antibodies against PGP9.5 a neuronal marker which decreased dramatically on the injured side consistent with the known loss and atrophy of axons in the CCI model.

Figure 7 Inhibition of STOML3 alleviates painful diabetic neuropathy

a, Diabetic peripheral neuropathy was induced using streptozotocin (STZ). After development of peripheral neuropathy, diabetic mice received a single injection of OB-1 or vehicle respectively into the plantar surface of the hind paw. **a,** Three hours after injection, OB-1 treated mice showed attenuated mechanical sensitivity displayed as percentage of withdrawal to increasing von Frey filaments. *** $p < 0.001$; Two-way ANOVA with $p > 0.0001$ ($F(1, 132) = 28{,}07$) OB-1 *vs*. STZ and Bonferroni's multiple comparison with $p > 0.9999$ ($t = 0{,}7867$ df = 132) (0.07g), $p > 0.9999$ ($t = 1.377$ df= 132) (0.16g), $p = 0.0033$ ($t = 3.539$ df= 132) (0.4g), $p = 0.0123$ ($t = 3.146$ df= 132) (0.6g), $p = 0.0404$ ($t = 2.753$ df= 132)

(1g), p > 0,9999, t = 1.377 df= 132 (1.4g) ; numbers indicate adult mice treated; data are displayed as mean of individual PWTs; error bars indicate s.e.m.) **b,** mechanical thresholds required to elicit 60% withdrawal frequency.** p < 0.01, *** p<0.001; (i) Wilcoxon Signed Rank Test with p = 0.0005 (Sum of signed ranks -78,00 Number of pairs 12, Naive *vs*. STZ, (ii) paired t-test, two-tailed with p = 0.0013 (t=4,287 df=11) STZ *vs*. STZ + OB1, p = 0.0004 (t=4,939 df=11) STZ + OB1 *vs*. OB-1 Wash-out; numbers indicate mice treated, two cohorts were tested independently; data are displayed as mean of individual PWTs; error bars indicate s.e.m.. **c,d**, Diabetic mice in the vehicle treated group showed no reversal of mechanical hypersensitivity. ** p < 0.01 (i) ordinary Two-way ANOVA with p = 0.0765 (F (1, 144) = 3,184) STZ vs. STZ+ Vehicle; (ii) Wilcoxon Signed Rank Test with p= 0.0765, Naive *vs*. STZ; (ii) paired t-test, two-tailed with p= 0.3125 (t=1,054 df=1) STZ *vs*. STZ + Vehicle, p=0.0859 (t=1,871 df=12) STZ + Vehicle *vs*. Vehicle Wash-out; numbers indicate mice treated from two cohorts tested independently; data are displayed as mean of individual PWTs; error bars indicate s.e.m.

Online Methods

The experiments in this study were carried out on adult inbred male or female mice (adult C57Bl/6n obtained from Charles River, Sulzfeld, Germany) or adult mice generated and breed in the laboratory (*Stoml3*$^{-/-}$, *Stoml3*^{StrepII} *or Stoml3*^{lacZ}). All experiments were performed in compliance with German and European laws for the use of animals in research and with appropriate permits from the Berlin authorities. Animals were kept under controlled temperature and a 12–h light, 12–h dark cycle with lights on at 06:00 A.M. Behavioral tests were conducted during the light phase. and the experimenter was blinded to treatment and genotype unless otherwise stated.

Statistics

All data were tested for normal distribution. Appropriate statistical tests applied for data analysis are referred to in the figure legend. Multiple comparisons were performed by repeated measures two-way ANOVA followed by Bonferroni post hoc test. Significance levels of $p < 0.05$ (*), $p < 0.01$ (**), and $p < 0.001$ (***) were used. Statistical analyses and exponential fits were made using the GraphPad Prism or Igor Pro 6.11. software. No statistical methods were used to pre-determine sample sizes but our sample sizes are similar to those reported in previous publications[1–11]. Experimenters were always blinded to treatment, or genotype unless otherwise stated. No special randomization procedures were used for assigning groups.

Molecular biology

Expression Constructs

Constructs for BiFC analysis were created by inserting the gene of interest, in frame, into the multiple cloning site of pBiFC-VC155 or pBiFC-VN173. Point mutations were introduced using PCR-based site-directed mutagenesis.

RT-PCR analysis

Lumbar L3-L6 dorsal root ganglia (DRG) were dissected from CCI and control mice, pooled and total RNA extracted with the TRIzol method (Invitrogen) as per manufacturer recommendations and treated with the TURBO DNA-free™ Kit to avoid DNA contamination. RNA was quantified using NanoDrop 2000 UV-Vis spectrophotometer (Thermo Scientific) and reverse-transcribed using SuperScript® III Reverse Transcriptase (Invitrogen). TaqMan Quantitative RT-PCR was used to detect the expression of STOML3 mRNA with 5´-GGAAGCCAGAGCCAAGGT-3´ and 5´-TGCAGGTACCGAAGTTGGA-3´primers in combination with the TaqMan probe #53 from Roche Universal Probe Library. Each sample was performed in triplicate in an ABI Prism 7700 Sequence Detection System (Thermo Scientific).

Cell culture

HEK-293 cells (passage numbers 4-20) were cultured in DMEM plus 10% fetal calf serum (FCS). Neuro2A (N2a) cells were cultured in DMEM/Opti-MEM media plus 10% FCS. Cell

lines were originally sourced from the ATCC and regularly checked for mycoplasma contamination. Sensory DRG neurons were isolated from 4 week old *Mus musculus* (C57Bl/6). Approximately 40 ganglia were collected from each mouse and individual cells were isolated by treating ganglia with 1 µg/ml collagenase IV for 30 min, followed by 1 ml of 0.05% trypsin, in PBS, for 5-20 min at 37°C. Enzyme-treated ganglia, in DMEM/F-12 media containing 10% Horse Serum (HS), were disrupted by gently passaging through a 20G needle; cells were then collected by centrifugation (1000 rpm, 3 min), washed and finally re-suspended in DMEM/F-12, 10% HS media (at no point were neurotrophins added to the culture). Experiments with isolated sensory neurons were conducted within 24-36 hours of isolation.

High through-put screen

HEK-293 cells were cultured to approximately 70% confluence; cells were co-transfected with plasmids encoding STOML3-VC and STOML3-VN using Fugene-HD, as per manufacturer's instructions. The transfection reaction proceeded for 8 h before cells were recovered and re-suspended in DMEM media containing 25 mM HEPES and lacking phenol red. Cells were plated on PLL-coated 384 well plates using an automated dispenser (EL406 Microplate Washer Dispenser). Plates already contained compounds from the ChemBioNet library (www.chembionet.info) a library containing small molecules with drug like properties[12]. Development of the YFP fluorescence signal was monitored overnight (15 h), with readings taken every 3 h (ex: 515 ± 8 nm, em: 535 ± 8 nm). Overnight monitoring of signal development was performed with a Freedom Evo workstation and a SafireII plate reader for fluorescence measurement (Tecan Group Ltd, Männedorf, Switzerland), and an integrated STX44-ICSA automated plate incubator (Liconic AG, Mauren, Liechtenstein). Experiments were repeated with 20 plates each day until the entire compound library had been screened and data was normalized to in-plate controls.

Compounds of interest were selected from the slope of YFP-signal vs time. Each well was compared to the average slope of in-plate positive controls (normalized percent activity), and compared to the mean and standard deviation of all samples on a plate (without the controls), giving a Z score as a measure of statistical significance[9]. One hundred and fifteen (115) inhibitors that significantly decreased the slope with a Z score < -3 were selected for further analysis. After re-screening in triplicate just 21 of the initially identified hit molecules were confirmed. Compounds that were themselves fluorescent or those that had significant effects on cell viability were discarded.

dSTORM imaging

N2a cells were cultured on EHS-Laminin coated precision coverglass, thickness 0.17mm, and transfected with a STOML3-FLAG plasmid. After overnight incubation, cells were treated for 3 hours with 20 µM compound, or DMSO as a control. Cells were fixed (15 min, 4% PFA), permeabilized (0.05% TritonX 100, 5 min) and blocked (phosphate buffered saline (PBS) containing 10% fetal goat serum (FGS), 37°C, 1 hr). Cells were labeled with mouse

anti-FLAG antibody (M2 clone Sigma #F1084, 1:100 in PBS containing 10% FGS). The secondary antibody was an Alexa647-conjugated, goat anti-mouse antibody (1:100 in PBS plus 10% FGS, 1 h, 37°C). After staining, the samples were fixed again. Prior to *d*STORM imaging, coverslips were mounted in *d*STORM buffer PBS, pH 7.4, containing an oxygen scavenger (0.5 mg/ml glucose oxidase), 40 mg/ml catalase, 10% (w/v) glucose and 100 mM MEA [13].

The custom-built *d*STORM system, based on a Nikon Ti microscope, was described in detail previously [14]. Before acquisition, we illuminated the Alexa647-labeled sample with 643 nm to switch fluorophores into the OFF state. After molecules started blinking, we acquired a sequence of frames (typically 10,000–20,000) using a 100x 1.49 NA objective, a 1.5 magnification lens and non-binned EMCCD array. An exposure time of 30 ms was used to ensure good signal-to-noise and a high number of blinking single molecules/frame.

In order to aid drift correction PLL-coated Tetra-speck fluorescent beads were allowed to adhere to the sample overnight. Localization: Single molecules were localized using open source software rapidSTORM 3.2 [15]. The source images are first smoothed via median operator followed by a fill-hole operation to reduce noise. In these 'de-noised' images, rapidSTORM performs a Gaussian fit (Levenberg–Marquardt parameter estimation) to each intensity spot, and fit quality and peak maxima were used as quality measures for localization. This fit yields the precise position of the single molecule with sub-pixel accuracy, the total intensity of the single molecule event and the frame number of the event. Sample drift was corrected using fiduciary beads in the sample as reference points (custom written algorithm, GREGOR).

For analysis of STOML3 domain size, all reconstructed images were blinded and then from each imaged cell 100 individual dots were cropped (size: 20 x 20 pixels). A 2D-Gaussian fit was calculated using the Igor software (WaveMetrics, USA). The x-width and y-width for each dot were included in the data set as domains were not necessarily circular.

Chemical Synthesis

The molecules OB-1 and OB-2 were structurally compared using a Tanimoto coefficient. The structures were translated with a FCFP-4 protocol and the resulting fingerprints did not show any significant similarity. Detailed chemical information for OB-1 and OB-2 can be found with the following links:

OB-1 http://www.chemspider.com/Chemical-Structure.948385.html

OB-2 http://www.chemspider.com/Chemical-Structure.9820833.html

For de novo synthesis 5.6 g of ethyl-3-oxo-3-phenylpropanoate (29.06 mmol) was solubilized in 50 ml toluene and 525 mg (1.45 mmol) of Cu(OTf)2 was added. Next, 1.57 g (14.5 mmol) of benzoquinone was solubilized in 20 ml of toluene and added dropwise to the reaction mixture followed by reflux for 3 h. The mixture was quenched with NH_4Cl and extracted three times with ethyl acetate. The combined organic layers were washed with brine and dried with Na_2SO_4. The crude product was purified by chromatography on silica gel eluting with a gradient of Hex/EE (10:1) to give 2.24 g of ethyl-5-hydroxy-2-phenylbenzofuran-3-carboxylate (Yield: 27 %) This product was an intermediate before final synthesis of OB-1. Next 0.5 g (1.77 mmol) of ethyl-5-hydroxy-2-phenylbenzofuran-3-carboxylate was

solubilized in 20 ml DMF and 1.2 eq Cs2CO3 (0.7 g, 2.1 mmol), 0.1 eq CuI (33 mg, 0.17 mmol) and 285 mg (1.77 mol) 5-chloro-1-mehtyl-4-nitro-1H-imidazole were added. The mixture was stirred for 3 h at room temperature. The organic solvent was removed under reduced pressure. The crude product was purified by chromatography on silica gel eluting with a gradient of Hex/EE (3:2) to give 644 mg of ethyl-5-(1-methyl-4-nitro-1H-imidazol-5-yloxy)-2-phenylbenzofuran-3-carboxylate (Yield: 89 %).

Electrophysiology

Whole-cell, patch-clamp recordings were conducted as previously described[2,10], using patch pipettes with a tip resistance of 3-6 MΩ, filled with a solution of: 110 mM KCl, 10 mM NaCl, 1mM MgCl2, 1 mM EGTA and 10 mM HEPES, adjusted to pH 7.3 with KOH. For experiments on DRG neurons 10 mM QX-314 was added to the pipette to block voltage-gated sodium channels[10]. Extracellular solutions contained 140 mM NaCl, 4 mM KCl, 2 mM $CaCl_2$, 1 mM $MgCl_2$, 4 mM glucose, 10 mM HEPES, adjusted to pH 7.4 with NaOH. A Zeiss 200 inverted microscope and an EPC-10 amplifier in combination with Patchmaster software was used, data was analyzed using Fitmaster software (HEKA Electronik GmbH, Germany). Mechanical stimuli were applied using a polished glass probe driven by the MM3A micromanipulator (Kleindiek Nanotechnik, Germany). Mechanical stimuli were applied by either; indenting the cell soma or by culturing cells on elastomeric pillar arrays and applying the stimulus to the cell-substrate interface by deflecting an individual pilus. For a detailed description of experiments using pillar arrays[10]. Images were obtained of the pilus before and after deflection and images were analyzed off-line to determine the exact deflection for each data point. Images were obtained using a 40x LD objective and a CoolSNAP EZ CCD camera. The collection of stimulus-response data using pillar arrays generates data sets with variation in both x and y. In order to effectively compare groups for each cell studied we binned response data by stimulus size in the following bins: 0-10, 10-50, 50-100, 100-250, 250-500, 500-1000 nm. For each cell, current amplitudes within each bin were averaged and then bins averaged between cells- we then tested for significance by testing whether the current amplitude for a given stimulation range (i.e. bin) differed between samples. To distinguish mechanoreceptors from nociceptors in the mixed population of acutely prepared DRG neurons, the shape of the generated action potential (AP) was used. For quantitative analysis of mechanosensitivity we measured responses in the most sensitive sub-population of mechanoreceptors with APs lacking a hump in the falling phase and a full width at half maximum (FWHM) of at least 0.7 ms, (average, ± s.e.m.: 0.9 ± 0.04 ms) [10].
To test the effect of compounds on stomatin modulation of ASIC currents CHO cells were transfected with vectors encoding Stomatin and ASIC3, in a ratio of 4:1 using lipofectamine, as per manufacturer's instructions. Cells were incubated with 20 μM OB-1 for 3 hours in extracellular buffer (see above), and OB-1 was maintained in the media during electrophysiological experiments. ASIC3 channels were gated by applying solutions of pH6 and pH4, and both the transient and sustained peak current density was measured.

Ex vivo skin nerve preparation

The skin-nerve preparation was used essentially as previously described to record from single primary afferents[7]. For the electrical search protocol a microelectrode (1MΩ) was maneuvered to contact the epineurium of the nerve trunk and an electrical stimulation was delivered at 1 s intervals with square wave pulses of 50 – 500 ms duration. In most filaments 3-5 single units were counted. The electrical nerve stimulation was done at 2 distant sites of the saphenous nerve to trace electrically identified units to their receptive fields. Mechanical sensitivity of single units was tested by mechanical stimulation with a glass rod. A computer-controlled nanomotor (Kleindiek, Reutlingen, Germany) was used to apply controlled displacement stimuli of known amplitude and velocity. The probe was a stainless steel metal rod and the diameter of the flat circular contact area was 0.8 mm containing a force transducer (Kleindiek, Reutlingen, Germany). The signal driving the movement of the linear motor and raw electrophysiological data were collected with a Powerlab 4.0 system (ADInstruments) and spikes were discriminated off-line with the spike histogram extension of the software.

Tactile perception task

Male C57Bl6/J mice were anaesthetized and a lightweight metal headholder was implanted to the skull using glue (Loctite 401, Henkel) and dental cement (Paladur®, Heraeus). Mice were habituated to the head-restraint and the behavioral setup over 1-2 days. Mouse licking and forepaw behavior was monitored with three custom-made capacitance sensors: a licking sensor, a rest sensor and a target sensor that provided an online monitor of paw or tongue contact. The rest sensor was a ball (diameter: 6 mm) mounted on a glass rod of 30 mm length, glued to a piezoelectric bender (PICMA® Multilayer Piezo Bender Actuator, Physik Instrumente). The piezo generated a 30 ms cosine tactile pulse via a piezo amplifier system (Sigmann Elektronik). The stimulus amplitude was calibrated with a high-speed (300 Hz) camera (Dalsa Genie HM640). The target sensor (diameter: 6 mm) had a start position of 10 mm horizontally in front of the rest sensor and was attached to a Fisso 3D articulated arm on a linear translation stage (ST9-100-2 eco-P, ITK Dr. Kassen GmbH, Germany). Mice were water restricted and given approximately 4 x 0.6 µl water rewards on condition of touching the target sensor within a defined latency from stimulus onset and licking the water dispenser. The target sensor moved to the start position at the start of a new trial and away from the mouse at the end of the trial. Inter-trial interval was randomized between 7 and 13 s. White noise was played throughout the trial. The response window (rewarded stimulus-to-touch latency) was reduced during behavioral training to 500 ms during the testing session. Mice were trained with high amplitude stimuli (620 µm) and then tested in the same session with seven different stimulus amplitudes (in µm: 45, 80, 125, 170, 275, 385, 620) and a no-stimulus trial to calculate the false alarm rate. Stimuli were presented in a randomized order. The setup was controlled with custom written software in LabView 10.0 (National Instruments 2010). Drug injections of OB-1 or DMSO alone were dissolved in Ringer's solution (in mM: 135 NaCl, 5 KCl, 5 HEPES, 1.8 CaCl2, 1 MgCl2) to make the OB-1 and vehicle solution. Approximately 5 µl was injected into the digits with a glass micropipette and 10 µl into the palm with a Hamilton syringe. During the injection procedure, the mouse

was anaesthetized with isoflurane (1.5 to 2.0 % in O2). The experimenter was not blinded to treatment.

To construct the psychometric curves we first averaged the rates of pressing the target sensor within 500 ms from stimulus onset across 5 mice. Next we fitted the data with a sigmoid function in Igor Pro 6.11 (WaveMetrics):

$$f(x) = base + \frac{max}{1+\exp(\frac{xY50-x}{slope})}$$

Mouse Pain Models and Behavioral Experiments

Chronic Constriction Injury

In deeply anaesthetized mice using isoflurane delivered in 100% O_2 (Univentor 410 Anaesthesia unit; Univentor, Malta), four loose silk (5/0; Catgut GmbH Markneukirchen) ligatures were placed around the sciatic nerve at the level of the right mid-thigh as described previously[5].

Spared Nerve Injury

In deeply anesthetized mice (see above) a skin and muscle incision was made at the thigh to reveal the sciatic trifurcation. Distal to the sciatic's trifurcation, nerve pieces (2-4 mm) of the sural as well as the common peroneal nerves were removed leaving the tibial nerve intact. In sham controls the surgery was performed without transecting the nerves. Wounds were closed with wound clips before anesthesia was terminated.

NGF-induced Hyperalgesia

A single dose of NGF (1 µg/g body weight) was injected intraperitoneal (i.p.) into adult mice and behavioral testing was performed 6h, 24h, 48h, and 72 hours post injection.

Diabetic Neuropathy Model

Eight week old C57Bl/6 mice were used for diabetes experiments. Diabetes was induced using previously reported protocols [11,16]. Briefly, 6 consecutive intraperitoneal injections of streptozotocin (STZ, Sigma-Aldrich, # S0130) were given with 24h intervals at 60 mg/Kg body weight in citrate buffer (0.05 M, pH 4.5) to induce diabetes. Blood glucose was maintained between 400 and 500 mg/dL throughout the experimental period. Mechanical sensitivity was measured and only those mice showing increased sensitivity to von Frey filaments as compared to basal sensitivity were selected for OB-1 testing. Vehicle or OB-1 (approximately 20 µl solution, 250 pmol per paw) was injected subcutaneously into intraplantar surface of diabetic mice under mild isoflurane anesthesia and mechanical sensitivity was measured from both injected (ipsilateral) and non-injected (contralateral) paws at 4 and 24h post-injection.

Assessing pain behavior.

Mice were allowed to habituate to the testing apparatus (acrylic chambers 10 × 10 cm in size, suspended above a wired mesh grid) one hour prior to behavioral testing. Calibrated von-Frey

hair monofilaments (Aesthesio® set of 20 monofilaments, Ugo Basil) were applied to the plantar surface of the hind paw in order to deliver target forces from 0.008 grams to 4 grams increasing in an approximately logarithmic scale. A single von Frey stimulus lasted for two seconds unless the mouse withdrew its paw. The up-and-down method described by Chaplan [8] was adapted as follows: Testing began with a 0.4 g filament applied three times A positive response was noted if paw withdrawal was seen to all three stimuli, so that the next smallest filament was tested next. A negative response was noted when paw withdrawal was not seen to at least one stimulus which was followed by testing with the next largest filament. Paw withdrawal thresholds were calculated as the median of 23 to 30 determined turning points.

A focused, radiant heat light source (IITC Life Science Inc.) was used to measure paw withdrawal thresholds to heat as previously described. The light beam created a focused spot of 4x6 mm on the hind paw. The time to paw withdrawal in response to a constantly increasing heat stimulus (maximal active intensity = 25% of the light source) with a cutoff of 20 seconds was determined. Heat stimuli were repeated 6 times for each paw with a stimulus interval of 1 minute.

Generation of Stoml3^{LacZ} and Stoml3^{StrepII} mice

The C57BL/6J mouse BAC clones (https:bacpac.chori.org) containing the *Stoml3* gene was isolated from RPCI-23 library[17]. A 12-kb DNA fragment containing the exon1 and its flanking regions of *Stoml3* gene was isolated by gap repair[18]. Homologous recombination in bacteria [18,19] was used to fuse an NLS-lacZ cassette to the ATG of *Stoml3* and to introduce the self-excision neo cassette [20] into the *Stoml3* locus. Similarly, homologous recombination in bacteria was used to introduce a Strep-TagII after the ATG of *Stoml3* and a neomycin cassette flanked by two loxP into the first intron of *Stoml3* locus to generate the *Stoml3^{StrepII}* allele. In both targeting vectors the MC1-diphteria toxin A (DTA) cassette was placed at the 3' end of the vector and was used for negative selection. Colonies of the E14.1 ES cell line (129/Ola) that had incorporated the targeting vector into their genome were selected by G418 and analyzed for homologous recombination by Southern blot analysis using 5' and 3' probes that lie outside of the targeting vector. Two clones were microinjected into C57BL/6 blastocysts to generate chimeras that transmitted the *Stoml3^{LacZ}* allele or the *Stoml3^{StrepII}* allele.

The *Stoml3^{LacZ}* strain was genotyped using Stoml3-LacZ F: gac agt gtg atg tca ggg aag; LacZ int R: cct tcc tgt agc cag ctt tca tc, Stoml3-LacZ R: cct tgt aaa ctg ata gcg ggg ac primers. The *Stoml3^{StrepII}* strain was genotyped using Stoml3-Strep F: gta gca gtg ttg ttt aga aag together with Stoml3-StrepII R2 gct agc cat ggc tca ttc ttg for the mutant allele or with Stoml3-Strep R1 aca gtg atg atg tcc cag c for the wild type allele.

The *Stoml3^{StrepII}* allele could conceivably negatively alter the function of the STOML3 protein. We thus generated homozygous *Stoml3$^{StrepII/StrepII}$* mice and used the ex vivo skin nerve preparation to determine if cutaneous mechanorecpetors lose mechanosensitivity in this strain. Recordings from 4 wild type littermate controls and 4 *Stoml3$^{StrepII/StrepII}$* mice revealed

no significant differences in the incidence of mechanoinsensitive fibers between the genotypes. Amongst Aβ-fibers mechanoinsensitive fiber incidence was 1/21 (5%) and 0/23 (0%) for wild type and *Stoml3*$^{StrepII/StrepII}$ mice respectively Amongst Aδ-fibers mechanoinsensitive fiber incidence was 0/12 (0%) and 1/11 (9%) for wild type and Stoml3$^{StrepII/StrepII}$ mice, respectively.

Histochemistry

Mice were perfused with ice-cold PBS followed by 0.5% gluteraldehyde for 20 minutes. Post-fixed lumbar DRGs were washed several times in PBS and cryoprotected in 30% sucrose overnight at 4°C. DRGs were embedded in O.C.T. Tissue-Tek (Sakura Finetek, Netherland) on dry ice and stored at -80°C. Tissue was on a Cryostat CM3050S (Leica) and slides were incubated in X-gal reaction buffer (35 mM potassium ferrocyanide, 35 mM potassium ferricyanide, 2mM MgCl2, 0.02% Nonidet P-40, 0.01% Na deoxycholate and 1 mg/ml of X-Gal) for 2 days at 37°. Slices were washed several times in PBS until the solution no longer turned yellow, air-dried and sealed with a coverslip.
Sections were observed on a Zeiss Axiovert 135 microscope using Zen imaging software (Zeiss, Germany). Image J (NIH, USA) was used to manually trace the outlines of cell in order to obtain cell area. Electron microscopy was performed on nerves using standard methods as previously described[7].

Western blotting

Tissues from *Stoml3*$^{StrepII/StrepII}$ and control mice were lysed with 8 M urea buffer and protein concentration was determined using the Bradford reagent. Proteins were separated by SDS-PAGE, followed by Western blot analysis using mouse Strep-tagII antibody (2-1507-001, IBA), PGP 9.5 antibody (ab10404, Abcam) and mouse anti β actin (A1978, Sigma). Appropriate horseradish peroxidase-conjugated secondary antibodies were used for chemiluminescence (ECL, Millipore or Supra, Thermo scientific SuperSignal).

Methods only references

1. Lechner, S. G. & Lewin, G. R. Peripheral sensitisation of nociceptors via G-protein-dependent potentiation of mechanotransduction currents. *J. Physiol.* **587,** 3493–3503 (2009).
2. Chiang, L.-Y. *et al*. Laminin-332 coordinates mechanotransduction and growth cone bifurcation in sensory neurons. *Nat. Neurosci.* **In Press,**
3. Hu, J. & Lewin, G. R. Mechanosensitive currents in the neurites of cultured mouse sensory neurones. *J. Physiol.* **577,** 815–828 (2006).
4. Brand, J. *et al*. A stomatin dimer modulates the activity of acid-sensing ion channels. *EMBO J.* **31,** 3635–3646 (2012).
5. Wetzel, C. *et al*. A stomatin-domain protein essential for touch sensation in the mouse. *Nature* **445,** 206–209 (2007).
6. Lechner, S. G., Frenzel, H., Wang, R. & Lewin, G. R. Developmental waves of mechanosensitivity acquisition in sensory neuron subtypes during embryonic

development. *EMBO J*. **28,** 1479–1491 (2009).
7. Moshourab, R. A., Wetzel, C., Martinez-Salgado, C. & Lewin, G. Stomatin-domain protein interactions with acid sensing ion channels modulate nociceptor mechanosensitivity. *J*. *Physiol*. (2013). doi:10.1113/jphysiol.2013.261180
8. Chaplan, S. R., Bach, F. W., Pogrel, J. W., Chung, J. M. & Yaksh, T. L. Quantitative assessment of tactile allodynia in the rat paw. *J*. *Neurosci*. *Methods* **53,** 55–63 (1994).
9. Brideau, C., Gunter, B., Pikounis, B. & Liaw, A. Improved statistical methods for hit selection in high-throughput screening. *J*. *Biomol*. *Screen*. **8,** 634–647 (2003).
10. Poole, K., Herget, R., Lapatsina, L., Ngo, H.-D. & Lewin, G. R. Tuning Piezo ion channels to detect molecular-scale movements relevant for fine touch. *Nat*. *Commun*. **5,** 3520 (2014).
11. Bierhaus, A. *et al*. Methylglyoxal modification of Nav1.8 facilitates nociceptive neuron firing and causes hyperalgesia in diabetic neuropathy. *Nat*. *Med*. **18,** 926–933 (2012).
12. von Kleist, L. *et al*. Role of the Clathrin Terminal Domain in Regulating Coated Pit Dynamics Revealed by Small Molecule Inhibition. *Cell* **146,** 471–484 (2011).
13. Heilemann, M. *et al*. Subdiffraction-resolution fluorescence imaging with conventional fluorescent probes. *Angew*. *Chem*. *Int*. *Ed*. *Engl*. **47,** 6172–6176 (2008).
14. Lampe, A., Haucke, V., Sigrist, S. J., Heilemann, M. & Schmoranzer, J. Multi-colour direct STORM with red emitting carbocyanines. *Biol*. *Cell* **104,** 229–237 (2012).
15. Wolter, S. *et al*. rapidSTORM: accurate, fast open-source software for localization microscopy. *Nat*. *Methods* **9,** 1040–1041 (2012).
16. Vareniuk, I., Pavlov, I. A. & Obrosova, I. G. Inducible nitric oxide synthase gene deficiency counteracts multiple manifestations of peripheral neuropathy in a streptozotocin-induced mouse model of diabetes. *Diabetologia* **51,** 2126–2133 (2008).
17. Osoegawa, K. *et al*. Bacterial artificial chromosome libraries for mouse sequencing and functional analysis. *Genome Res*. **10,** 116–128 (2000).
18. Lee, E. C. *et al*. A highly efficient Escherichia coli-based chromosome engineering system adapted for recombinogenic targeting and subcloning of BAC DNA. *Genomics* **73,** 56–65 (2001).
19. Liu, P., Jenkins, N. A. & Copeland, N. G. A highly efficient recombineering-based method for generating conditional knockout mutations. *Genome Res*. **13,** 476–484 (2003).
20. Bunting, M., Bernstein, K. E., Greer, J. M., Capecchi, M. R. & Thomas, K. R. Targeting genes for self-excision in the germ line. *Genes Dev*. **13,** 1524–1528 (1999).

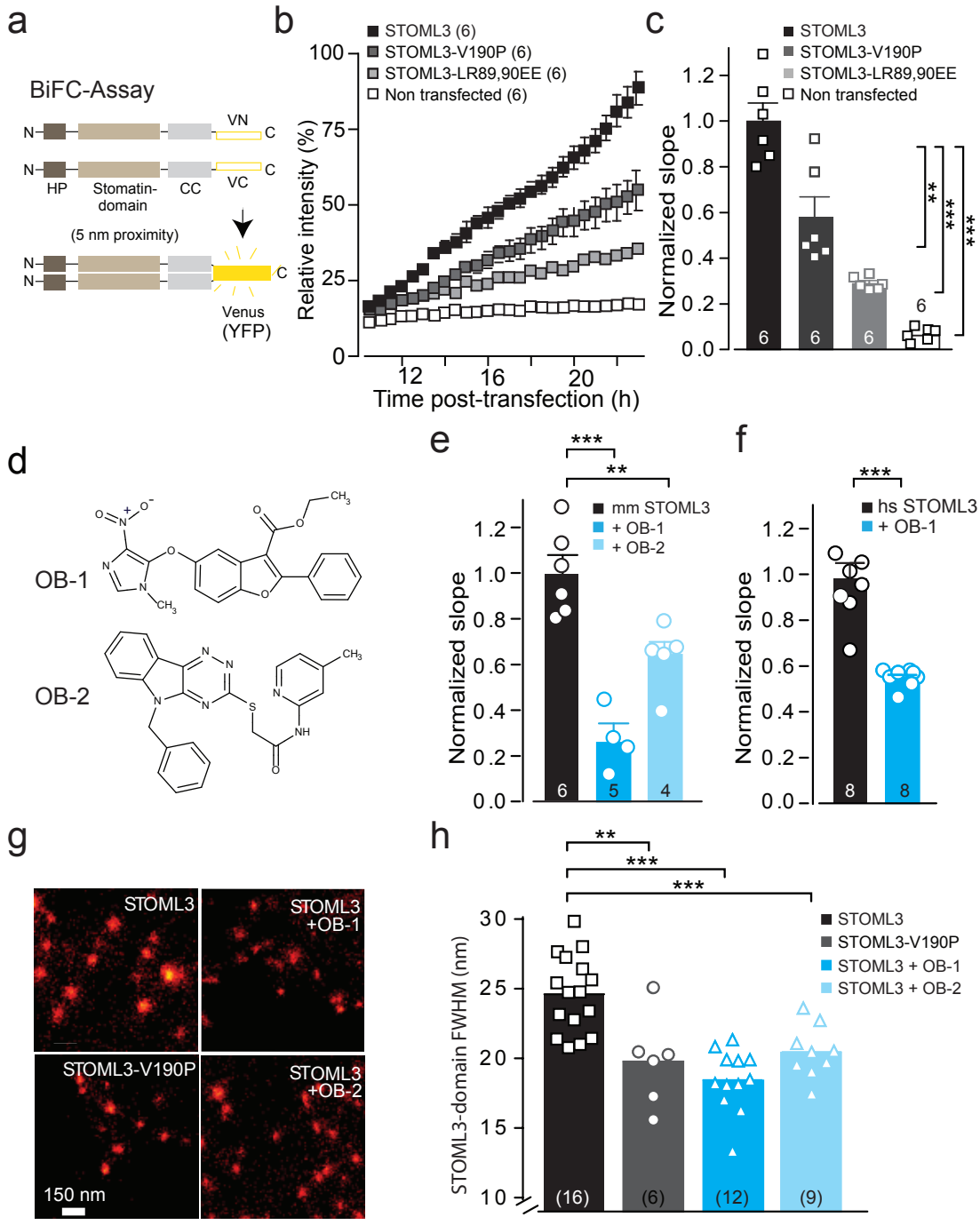
a
BiFC-Assay
VN
VC
HP
Stomatin-domain
CC
(5 nm proximity)
Venus (YFP)
b
STOML3 (6)
STOML3-V190P (6)
STOML3-LR89,90EE (6)
Non transfected (6)
Relative intensity (%)
Time post-transfection (h)
c
STOML3
STOML3-V190P
STOML3-LR89,90EE
Non transfected
Normalized slope
d
OB-1
OB-2
e
mm STOML3
+ OB-1
+ OB-2
Normalized slope
f
hs STOML3
+ OB-1
Normalized slope
g
STOML3
STOML3 +OB-1
STOML3-V190P
STOML3 +OB-2
150 nm
h
STOML3
STOML3-V190P
STOML3 + OB-1
STOML3 + OB-2
STOML3-domain FWHM (nm)

Figure 1

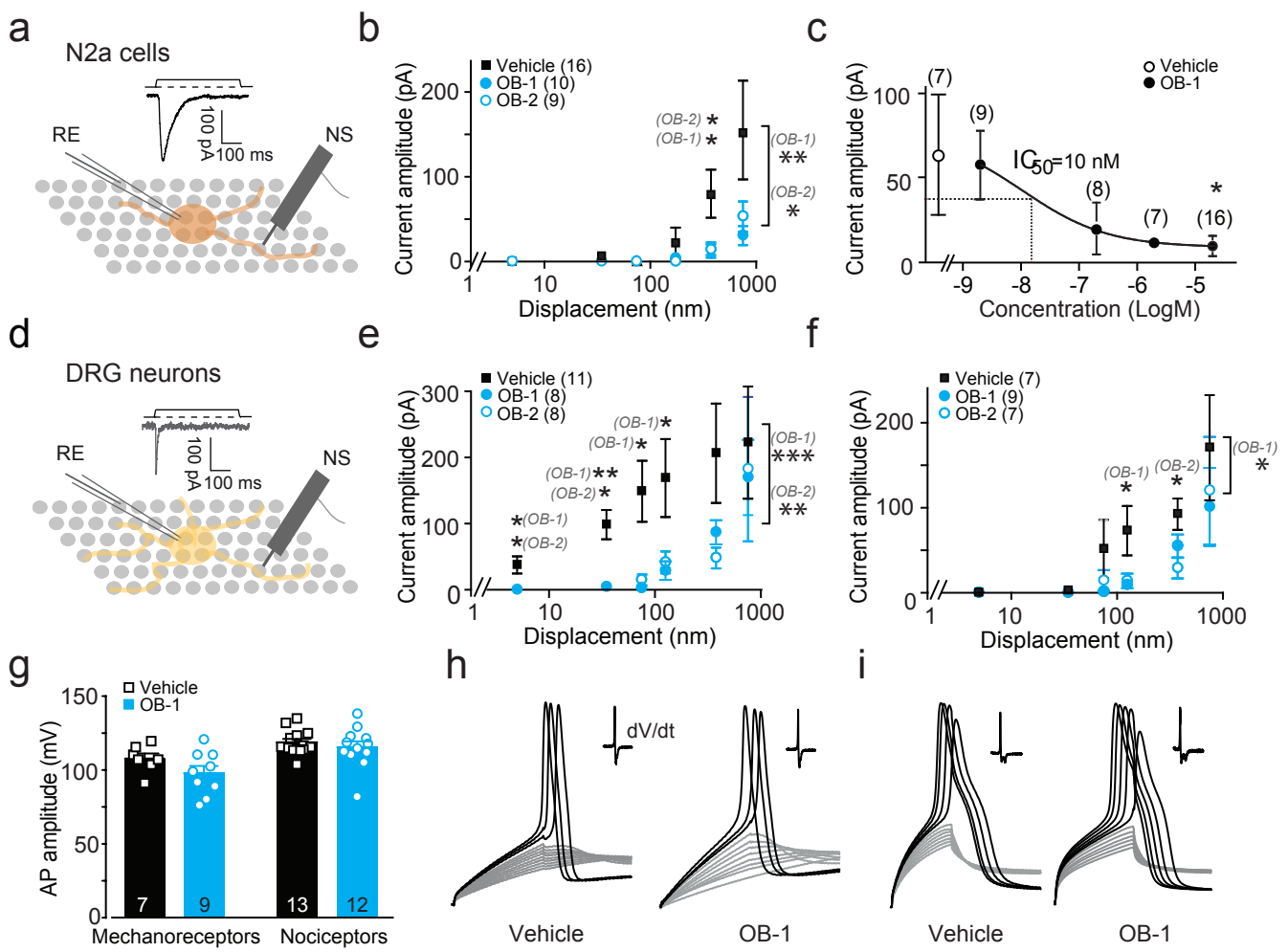
a
N2a cells
RE
NS
100 pA
100 ms
b
Vehicle (16)
OB-1 (10)
OB-2 (9)
Current amplitude (pA)
Displacement (nm)
(OB-2) *
(OB-1) *
(OB-1) **
(OB-2) *
c
Vehicle
OB-1
IC50=10 nM
Current amplitude (pA)
Concentration (LogM)
(7)
(9)
(8)
(7)
(16)
*
d
DRG neurons
RE
NS
100 pA
100 ms
e
Vehicle (11)
OB-1 (8)
OB-2 (8)
Current amplitude (pA)
Displacement (nm)
*(OB-1)
*(OB-2)
(OB-1)**
(OB-2)*
(OB-1)*
(OB-1)*
(OB-1) ***
(OB-2) **
f
Vehicle (7)
OB-1 (9)
OB-2 (7)
Current amplitude (pA)
Displacement (nm)
(OB-1) *
(OB-2) *
(OB-1) *
g
Vehicle
OB-1
AP amplitude (mV)
7
9
13
12
Mechanoreceptors
Nociceptors
h
dV/dt
Vehicle
OB-1
i
Vehicle
OB-1

Figure 2

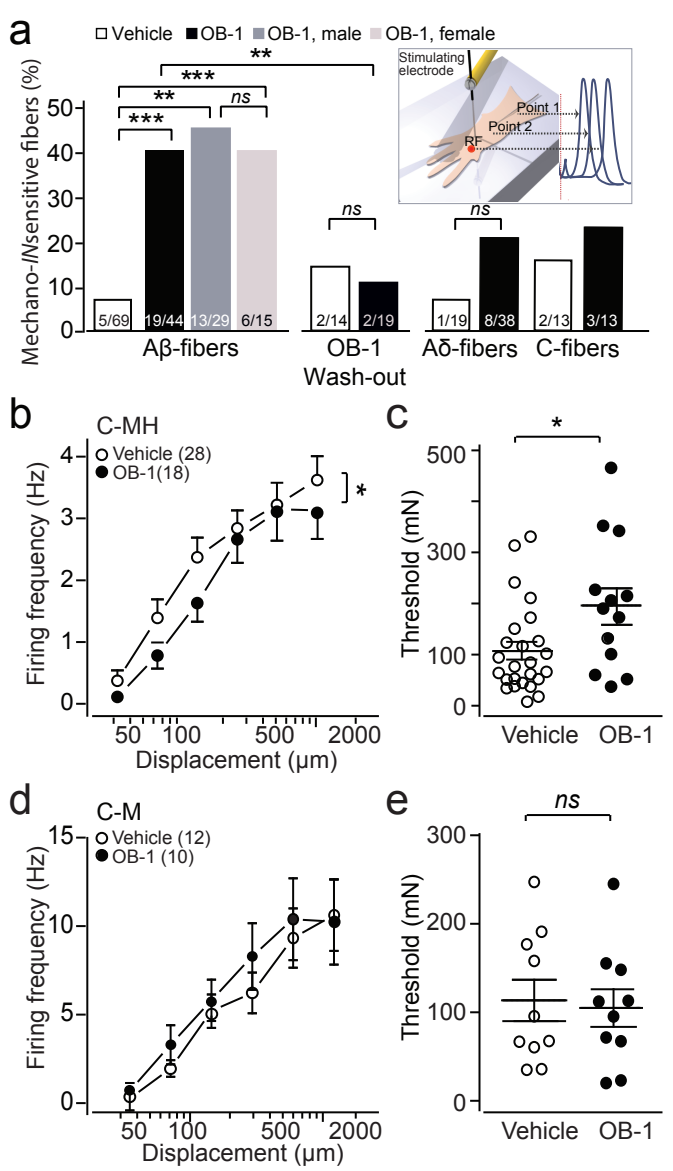
a
Vehicle
OB-1
OB-1, male
OB-1, female
Mechano-/Nsensitive fibers (%)
Stimulating electrode
Point 1
Point 2
RF
5/69
19/44
13/29
6/15
2/14
2/19
1/19
8/38
2/13
3/13
Aβ-fibers
OB-1 Wash-out
Aδ-fibers
C-fibers
b
C-MH
Vehicle (28)
OB-1(18)
Firing frequency (Hz)
Displacement (μm)
c
Threshold (mN)
Vehicle
OB-1
d
C-M
Vehicle (12)
OB-1 (10)
Firing frequency (Hz)
Displacement (μm)
e
Threshold (mN)
Vehicle
OB-1

Figure 3

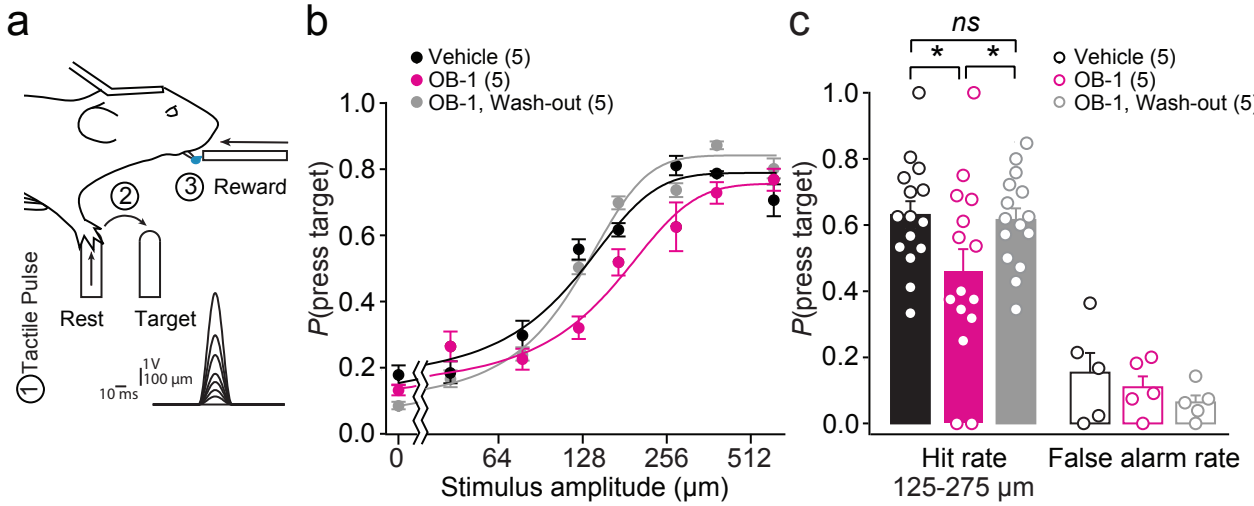
a
b
c
Tactile Pulse
Rest
Target
Reward
1V
100 µm
10 ms
Vehicle (5)
OB-1 (5)
OB-1, Wash-out (5)
P(press target)
Stimulus amplitude (µm)
ns
Hit rate
125-275 µm
False alarm rate

Figure 4

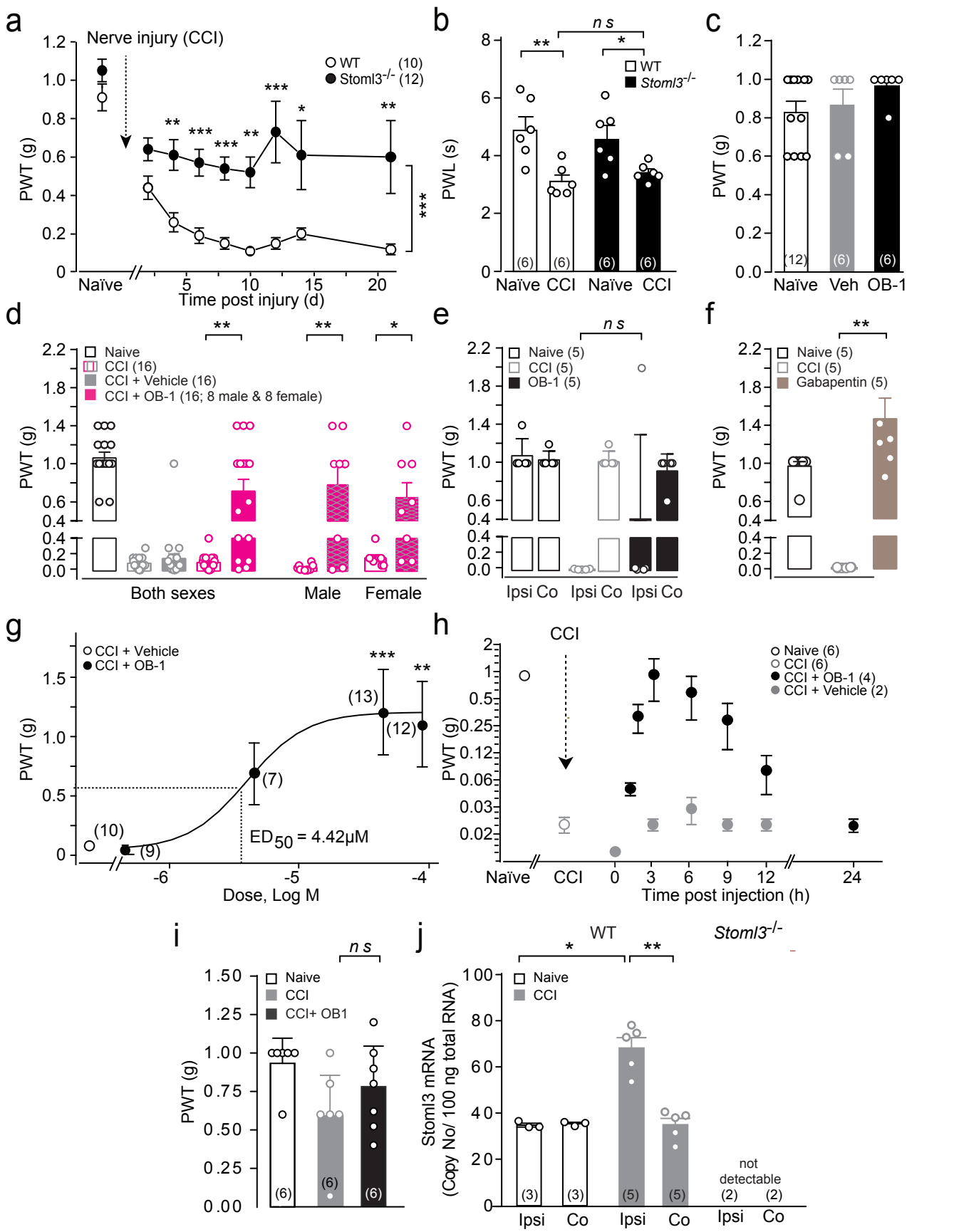
a
Nerve injury (CCI)
WT (10)
Stoml3-/- (12)
PWT (g)
Naïve
Time post injury (d)
b
n s
PWL (s)
WT
Stoml3-/-
Naïve CCI Naïve CCI
c
PWT (g)
Naïve Veh OB-1
d
Naive
CCI (16)
CCI + Vehicle (16)
CCI + OB-1 (16; 8 male & 8 female)
PWT (g)
Both sexes
Male
Female
e
n s
Naive (5)
CCI (5)
OB-1 (5)
PWT (g)
Ipsi Co Ipsi Co Ipsi Co
f
Naive (5)
CCI (5)
Gabapentin (5)
PWT (g)
g
CCI + Vehicle
CCI + OB-1
PWT (g)
ED50 = 4.42μM
Dose, Log M
h
CCI
Naive (6)
CCI (6)
CCI + OB-1 (4)
CCI + Vehicle (2)
PWT (g)
Naïve CCI
Time post injection (h)
i
n s
Naive
CCI
CCI+ OB1
PWT (g)
j
WT
Stoml3-/-
Naive
CCI
Stoml3 mRNA
(Copy No/ 100 ng total RNA)
not detectable
Ipsi Co Ipsi Co Ipsi Co

Figure 5

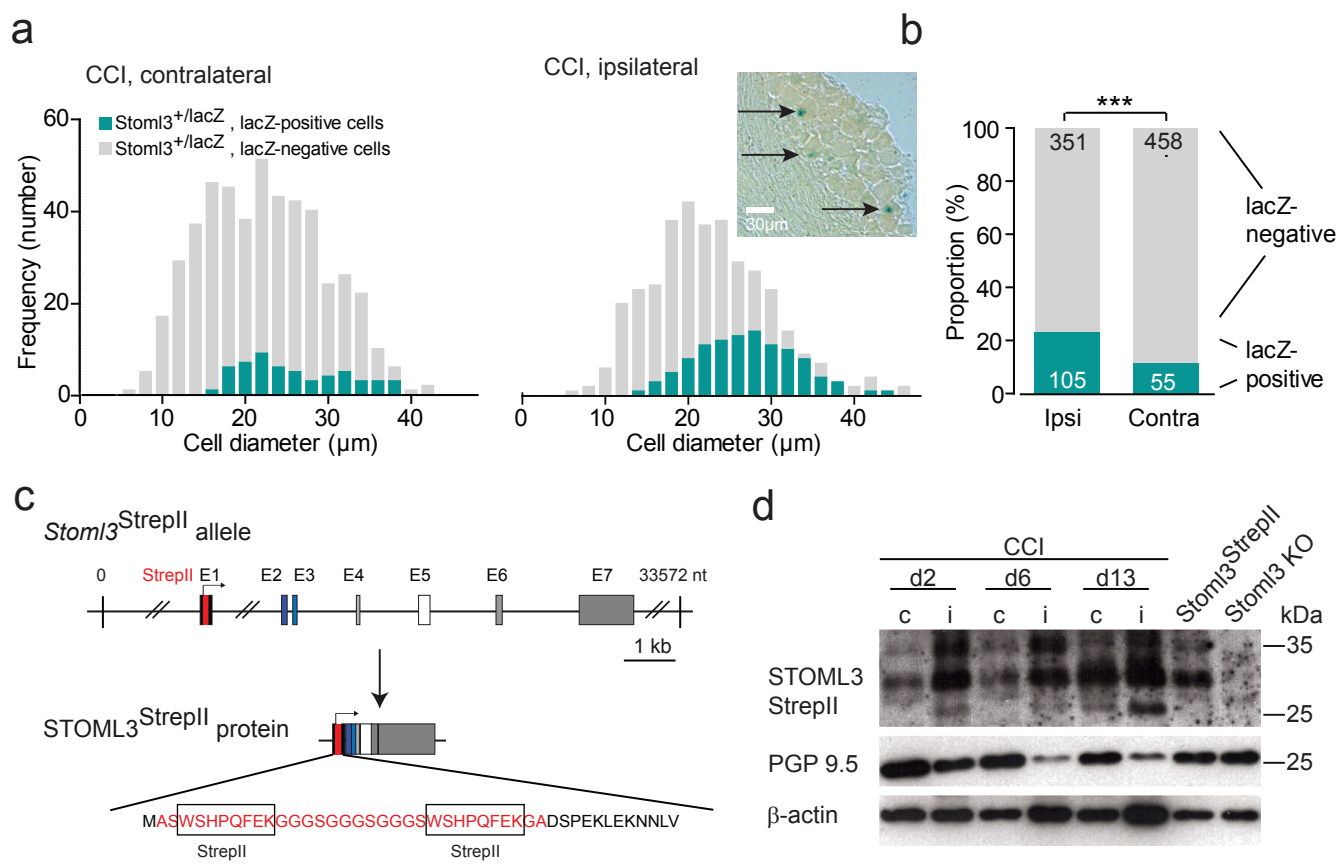
a
CCI, contralateral
Stoml3+/lacZ , lacZ-positive cells
Stoml3+/lacZ , lacZ-negative cells
Frequency (number)
Cell diameter (μm)
CCI, ipsilateral
30μm
b
***
351
458
105
55
Proportion (%)
Ipsi
Contra
lacZ-negative
lacZ-positive
c
Stoml3StrepII allele
0
StrepII
E1
E2
E3
E4
E5
E6
E7
33572 nt
1 kb
STOML3StrepII protein
MASWSHPQFEKGGGSGGGSGGGSWSHPQFEKGADSPEKLEKNNLV
StrepII
StrepII
d
CCI
d2
d6
d13
c
i
Stoml3StrepII
Stoml3 KO
kDa
STOML3 StrepII
PGP 9.5
β-actin
35
25
25

Figure 6

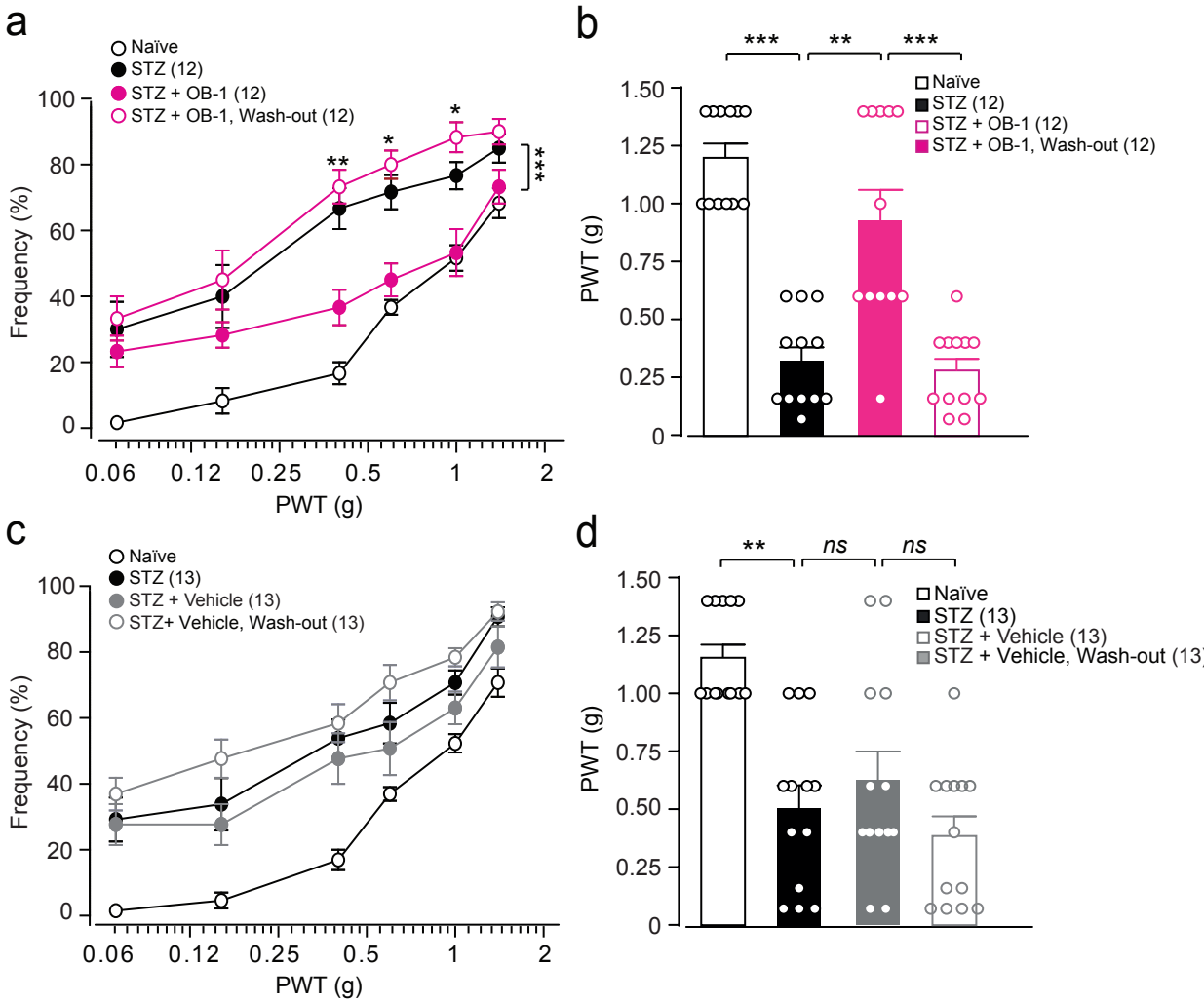
a
Naïve
STZ (12)
STZ + OB-1 (12)
STZ + OB-1, Wash-out (12)
Frequency (%)
PWT (g)
0.06
0.12
0.25
0.5
1
2
b
Naïve
STZ (12)
STZ + OB-1 (12)
STZ + OB-1, Wash-out (12)
PWT (g)
c
Naïve
STZ (13)
STZ + Vehicle (13)
STZ+ Vehicle, Wash-out (13)
Frequency (%)
PWT (g)
d
Naïve
STZ (13)
STZ + Vehicle (13)
STZ + Vehicle, Wash-out (13)
PWT (g)
ns

Figure 7